Ollscoil na Gaillimhe
University of Galway

Provided by the author(s) and University of Galway in accordance with publisher policies. Please cite the published version when available.

Title	Combustion of n-C3–C6 linear alcohols: An experimental and kinetic modeling study. Part I: Reaction classes, rate rules, model lumping, and validation
Author(s)	Pelucchi, M.; Namysl, S.; Ranzi, E.; Rodriguez, A.; Rizzo, C.; Somers, K. P.; Zhang, Y.; Herbinet, O.; Curran, Henry J.; Battin-Leclerc, F.; Faravelli, T.
Publication Date	2020-10-27
Publication Information	Pelucchi, M., Namysl, S., Ranzi, E., Rodriguez, A., Rizzo, C., Somers, K. P., Zhang, Y., Herbinet, O., Curran, H. J., Battin-Leclerc, F., Faravelli, T. (2020). Combustion of n-C3–C6 Linear Alcohols: An Experimental and Kinetic Modeling Study. Part I: Reaction Classes, Rate Rules, Model Lumping, and Validation. Energy & Fuels, 34(11), 14688-14707. doi:10.1021/acs.energyfuels.0c02251
Publisher	American Chemical Society
Link to publisher's version	https://doi.org/10.1021/acs.energyfuels.0c02251
Item record	http://hdl.handle.net/10379/16486
DOI	http://dx.doi.org/10.1021/acs.energyfuels.0c02251

Downloaded 2024-04-19T20:48:24Z

Some rights reserved. For more information, please see the item record link above.

Combustion of *n*-C_3–C_6 linear alcohols: an experimental and kinetic modeling study.

Part I: reaction classes, rate rules, model lumping and validation.

M. Pelucchi[1*], S. Namysl[2], E. Ranzi[1], A. Rodriguez[2], C. Rizzo[1], K. P. Somers[3], Y. Zhang[4],

O. Herbinet[2], H.J. Curran[3], F. Battin-Leclerc[2], T. Faravelli[1]

[1] *CRECK Modeling Lab, Department of Chemistry Materials and Chemical Engineering, Politecnico di Milano, 20133, Milano, Italy*

[2] *Laboratoire Réactions et Génie des Procédés, CNRS, Université de Lorraine, ENSIC, Nancy Cedex, France*

[3] *Combustion Chemistry Centre, National University of Ireland Galway, Galway, Ireland*

[4] *State Key Laboratory of Multiphase Flow in Power Engineering, Xi'an Jiaotong University, Xi'an 710049, China*

Corresponding author:

Dr. Matteo Pelucchi,
Department of Chemistry, Materials
and Chemical Engineering,
Politecnico di Milano, Milan, Italy
Email: matteo.pelucchi@polimi.it
Tel: +39 02 2399 4234

Keywords

n-C_3-C_6 alcohols, pyrolysis, combustion, rapid compression machine, jet-stirred reactor, kinetic model.

Abstract

This work (Part I and Part II) presents new experimental data for *n*-C_3 – C_6 alcohols combustion (*n*-propanol, *n*-butanol, *n*-pentanol, *n*-hexanol) and a lumped kinetic model to describe their pyrolysis and oxidation. The kinetic subsets for alcohol pyrolysis and oxidation from the CRECK kinetic model have been systematically updated to describe the pyrolysis and high and low temperature oxidation of this series of fuels. Using the reaction class approach, the reference kinetic parameters have been determined based on experimental, theoretical and kinetic modeling studies previously reported in the literature, providing a consistent set of rate rules allowing easy extension and good predictive capability. The modeling approach is based on the assumption of an alkane-like and an alcohol specific moiety for the alcohol fuel molecules. A thorough review and discussion of the information available in the literature supports the selection of the kinetic parameters that are then applied to the *n*-C_3 – C_6 alcohol series and extended for further proof to describe *n*-octanol oxidation. Due to space limitation, to the large amount of information and to the comprehensive character of this study the manuscript has been divided into two parts. Part I describes the kinetic model with the

lumping techniques and provides a synoptic synthesis of its wide range of validations made possible by newly obtained experimental data. These including speciation measurements carried out in a jet-stirred reactor (p = 107 kPa, T = 550 – 1100 K, φ = 0.5, 1.0, 2.0) for *n*-butanol, *n*-pentanol and *n*-hexanol and ignition delay times of ethanol, *n*-propanol, *n*-butanol, *n*-pentanol/air mixtures measured in a rapid compression machine at φ = 1.0, p = 10 and 30 bar, and T = 704 – 935 K are presented in Part II, together with their comparison with predictions using the new model and a detailed kinetic discussion. This work provides new experimental targets that are useful for kinetic model development and validation (Part II), as well as an extensively validated kinetic model (Part I), containing also the subsets of other reference components for real fuels thus allowing the assessment of combustion properties of new sustainable fuels.

Outline

1. **Introduction**
2. **Kinetic model development: reaction classes and reference kinetic parameters**
3. **Lumping of the detailed kinetic mechanism**
4. **Preliminary model validation**
5. **Conclusions**

Acknowledgements

References

1. Introduction

Alcohols are promising alternative fuels from the perspective of carbon footprint reduction in the transport sector, as well as being blending fuel components for internal combustion engines. Alcohol based fuels have the potential to be used in a near CO_2-neutral way, through efficient conversion of ligno-cellulosic biomass [1, 2]. In spark ignition engines, the resistance to ignition, or the anti-knocking propensity, of a fuel is characterized by its octane rating that can be measured as the research octane number (RON) and/or the motor octane number (MON). As suggested by Kalghatgi et al. [3, 4], a better characterization can be obtained by combining the RON and MON to obtain the octane index, OI = RON – KS, where S is the octane sensitivity (S = RON – MON) and K an empirical parameter that depends on the pressure and temperature conditions of the engine. Commercial gasoline fuel RON and MON values are typically in the range of 90 – 100 and 82 – 90, respectively. The counterpart to the octane rating in compression ignition engines is the cetane number (CN), representing instead the propensity to ignition of a fuel, with commercial diesel fuels having CNs in the range 45 – 55.

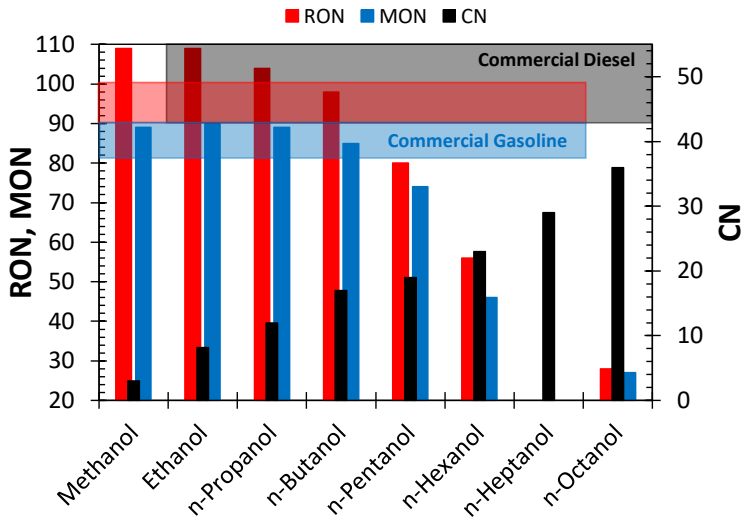

Figure 1: RON (red), MON (blue) and CN (black) values for methanol, ethanol and linear C_3–C_8 n-alcohols (bars) with that of commercial gasoline and diesel fuels (shaded areas) [5, 6]. Red shaded and blue shaded areas represent RON and MON ranges for commercial gasoline fuels. Black shaded area represents CN range for commercial diesel fuels.

Figure 1 compares the RON, MON and CN values for methanol, ethanol and linear *n*-C_3 – C_8 alcohols (bars) with those of commercial gasoline and diesel fuels (shaded areas), as reported by Sarathy et al. [5] and by the U.S. National Renewable Energy Laboratory-NREL [6]. Methanol, ethanol, propanol and butanol have

octane ratings comparable or higher than that of commercial gasoline fuels. In addition, their octane sensitivity (S = RON – MON), matches or exceeds that of commercial gasoline fuels (S ≈ 10), making them suitable for modern low temperature combustion (LTC) and direct injection spark ignition engines [7]. Higher molecular weight alcohols (≥ C_5) have lower knock resistance (i.e. a lower octane rating), thus preventing their blending with gasoline fuels. However, as the linear carbon chain length increases the cetane number also increases, approaching that of commercial diesels, making fuels like *n*-octanol highly suitable for compression ignition engines [8] or as blending components in jet engines. Even *n*-pentanol and *n*-hexanol have been successfully tested in diesel engines, both as neat fuels and in blends with commercial diesel or biodiesel fuels [9-16]. In relation to new engine technologies, a recent modeling study investigated the operability maps of *n*-butanol and *n*-pentanol in HCCI engines using a detailed kinetic model [17]. It was found that these fuels largely extend the operability maps towards lower engine loads and higher exhaust gas recirculation compared to primary reference fuels (PRFs) and toluene primary reference fuels (TPRFs) mixtures (RON/MON = 80 – 100).

The development of detailed and predictive combustion kinetic models provides a very efficient tool for the synergistic design of fuels and engines [18], allowing parametric analyses to explore, interpolate and extrapolate the propensity or the resistance to ignition of different fuels and fuel blends [19]. In general, the reactivity of oxygenated biofuels (e.g. alcohols, aldehydes, organic acids) is largely influenced by the presence of an oxygenated functional group that modifies bond dissociation energies and enhances, inhibits and triggers different reaction pathways compared to the parent fuel molecule (e.g. alkane) [20]. The recent interest in biofuels and bio-oils from the fast pyrolysis of biomass has motivated systematic experimental and modeling investigations of different chemical families such as aldehydes [21-25], acids [26] and oxygenated aromatics [27-29] to unravel the effects of different oxygenated functional groups on fuel kinetics. Beyond their application as surrogate fuel components [30], such species are also important intermediates in the oxidation of alternative or conventional hydrocarbon fuels, as they are implicit in the hierarchical nature of complex combustion kinetic models. These previous studies aimed to systematically assess the influence of the oxygenated moieties and to provide a set of consistent rate constants capable of

describing the different chemical pathways triggered by the different functions. The present work complements previous studies [21, 26] extending them to linear *n*-C_3–C_6 alcohols. As reviewed recently by Sarathy et al. [5], a great number of experimental and kinetic modeling studies on alcohols have been reported in the literature. In particular, many efforts have been devoted to the investigation of methanol, ethanol and the isomers of propanol, butanol and pentanol. Despite their importance, a more limited number of studies are available for longer chain alcohols such as *n*-hexanol and *n*-octanol.

Based on available theoretical [31-43] and experimental [44-49] rate constant determinations, as well as on previous comprehensive modeling studies [5, 50-55], this work provides a consistent set of rate constants to describe the pyrolysis and high and low temperature combustion mechanisms of *n*-C_3 – C_6 alcohols with specific attention paid to the impact of the hydroxyl functional group. The kinetic model thus obtained is validated by comparison with both the new ignition delay time and speciation measurements presented here and with other targets available in the literature. As a further proof of the validity of the approach and of the rate rules adopted, the model is successfully extended to describe *n*-octanol oxidation (see Part II [56]).

The manuscript is organized as follows. Section 2 presents the rate constants for the different reaction classes needed to describe the pyrolysis and oxidation of alcohols. The lumping approach to describe the low temperature combustion chemistry is discussed in Section 3. A synopsis of model validations and performances is presented in Section 4. For a more detailed discussion on model validations and performances the reader is referred to Part II of this study [56].

2. Kinetic Model Development

Models for *n*-C_3 – C_6 alcohols combustion were proposed in the literature [50-55, 57-61], with *n*-butanol being the most targeted fuel. After the detailed review by Sarathy et al. [5], Li et al. [54] proposed a kinetic model for pyrolysis and high temperature combustion of *n*-propanol and *iso*-propanol. A similar study on *n*-pentanol has been recently presented by Wang et al. [55]. Nativel et al. [53] recently measured laminar flame speed for *n*- and *iso*-pentanol, presenting a kinetic model for their high temperature oxidation. In the context

of the CRECK kinetic model, Frassoldati et al. [51] and Grana et al. [52] investigated the high temperature oxidation of propanol and the butanol isomers, respectively. The model was later extended to the pentanol isomers [53]. A lumped low temperature mechanism to describe *n*-butanol oxidation was proposed by Pelucchi et al. [20] and extended by analogy to *n*-pentanol to investigate the operability maps of a HCCI engine fueled with *n*-butanol and *n*-pentanol [17].

Motivated by the new measurements presented and discussed in Part II of this study [56] and by new experimental information presented in the literature since the last developments of the alcohols subset, this work presents an updated single comprehensive kinetic model for *n*-C_3 – C_6 alcohols pyrolysis and combustion. Different from the previous comprehensive model by Sarathy et al. [5], the lumping procedure applied to the low temperature oxidation and to the fuel radicals for higher molecular weight alcohols (C ≥ 5) allows the generation of a more compact kinetic model. In addition, to the authors knowledge, the attached kinetic model presents the first attempt to describe the oxidation of *n*-propanol under conditions different from pyrolysis or high temperature oxidation (T > 1000 K), despite the persisting scarcity of experimental data at lower temperatures.

2.1 Overview of the model development

Due to the interest in alcohols as blending components for commercial fuels, the CRECK model attached herein accounts for the combustion chemistry of a variety of species relevant to transportation fuels (gasoline, diesel, jet fuels, oxygenated fuels) as documented in detail in the periodically updated webpage [62]. The model can be also used to characterize the formation of pollutants such as polycyclic aromatic hydrocarbons leading to soot formation [63] and NOx [64]. At the core of the kinetic models is the AramcoMech1.3 $C_0 – C_2$ mechanism from [65, 66] and the C_3 subset from Burke et al. [67], including the methanol and ethanol subsets. Minor updates from [68] have been incorporated in the $C_0 – C_1$ chemistry. The comprehensive kinetic mechanism for high and low-temperature oxidation consists of 491 species and 17888 reactions and is attached as Supplementary material, together with the species nomenclature. Out of these, 37 species are used to describe the primary oxidation pathways of *n*-$C_3 – C_6$ alcohols. Taking advantage of the modular structure of the CRECK kinetic model, five versions of different size are attached as Supplementary

Material to this work (Table S1). These versions are obtained by including or excluding the kinetic subsets to describe the low temperature chemistry, NOx [64] and PAHs formation [63]. The thermodynamic properties have been adopted from ATcT tables [69, 70] (as in Bagheri et al. [68]) or from the work of Metcalfe et al. [65] and Burke et al. [67]. Thermodynamic properties for *n*-$C_3 - C_6$ alcohols are derived from group additivity [71] with updated values from Burke et al. [67]. Transport properties for alcohols and derived radicals are from previous kinetic studies [51-53, 61].

As previously discussed in the literature [50, 52, 53, 57-59, 72], it is convenient to treat the oxidation of higher molecular weight alcohols by coupling the specific features (i.e. reaction classes, rate rules, alternative pathways) of an alcohol moiety, influenced by the presence of the hydroxyl group (R–OH), and an alkane-like function. The same approach has been recently generalized for different oxygenated fuels [20], and applied to the systematic investigation of *n*-$C_4 - C_6$ aldehydes [21] and *n*-$C_4 - C_5$ organic acids [26]. In this work, the collection of theoretical and experimental information from the literature and a thorough assessment of different experimental targets permits the formulation of rules of general validity for the alcohol-specific moiety. The alkane-like moiety is treated according to rate rules already validated for *n*-alkanes [73, 74], also considering possible interactions with the alcohol-specific moiety (e.g. through isomerization reactions). Figure 2 supports the above assumptions showing bond dissociation energies (BDEs) at $T = 298$ K for different alcohol molecules, as reported in previous combustion kinetic studies [5, 50, 57, 75]. BDEs for methanol and ethanol are from the ATcT Tables [69, 70]. BDEs for *n*-hexanol are extrapolated from *n*-pentanol.

The different theoretical methods adopted for BDEs calculations (e.g. CBS-QB3, G4) in previous studies have comparable degrees of uncertainty (± 1.5 – 2.0 kcal mol^{-1}). More accurate calculations (i.e. ± 1.0 kcal mol^{-1}) have been reported in the systematic studies on oxygenated molecules by Oyeyemi et al. [76, 77]. Bar diagrams in Figure 2 compare BDEs by Oyeyemi et al. and from previous kinetic studies, averaged on the *n*-$C_3 - C_5$ alcohol series, with the values calculated from the thermochemical parameters of the kinetic model attached to this study. A generally good agreement is observed for C–H, O–H, C–C and C–O bond dissociation energies (< 2 kcal mol^{-1}). Maximum differences ≤ 1 kcal mol^{-1} are observed for C–H and O–H BDEs.

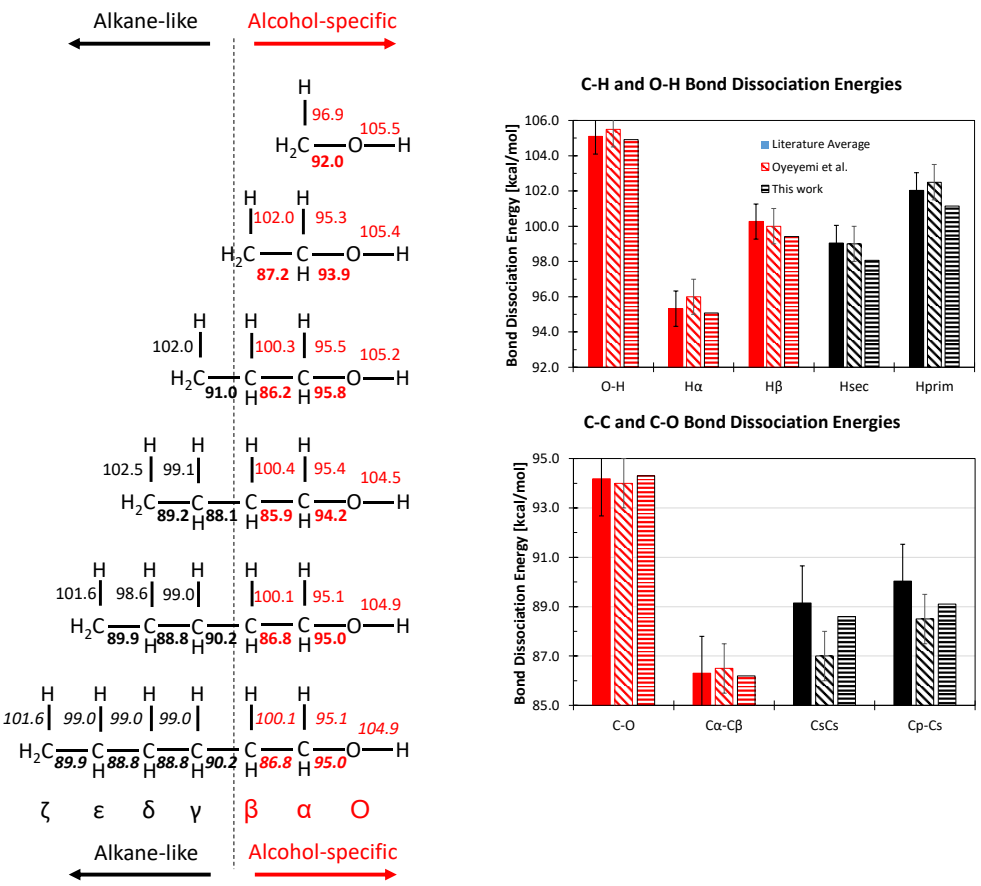

Figure 2: Left panel: bond dissociation energies (BDEs) for C-H bonds [5], and for C–C bonds (bold) [50, 57, 69, 70, 75]. BDEs for n-hexanol are derived from n-pentanol. Right panel: bar diagrams compare BDEs by Oyeyemi et al. [76, 77] (diagonal filling) and from previous kinetic studies (full bars), averaged on the n-C_3–C_5 alcohol series, with the values calculated from the thermochemical parameters of the kinetic model attached to this study (horizontal filling).

Starting from the alcohol-specific moiety, the hydroxyl function, O–H, has the strongest bond in alcohol fuel molecules. BDEs are in the range of 104 – 106 kcal mol^{-1}, with an average value of ≈ 105 kcal mol^{-1}. The electron withdrawing hydroxyl moiety strongly reduces the bond dissociation energy of the secondary C–H bond in the α position (≈ 95 kcal mol^{-1}), compared to typical values of secondary C–H bonds in alkanes (BDE ≈ 98.5 kcal mol^{-1}). The presence of the hydroxyl function also influences the strength of the secondary C–H bond in the β position, where the average value of ≈ 100 kcal mol^{-1} is 1 – 2 kcal mol^{-1} higher than a secondary C–H in corresponding alkanes. From the γ position onward, it is widely assumed that the influence of the oxygenated function disappears [20]. BDEs for secondary (≈ 98.5 kcal mol^{-1}) and primary (≈ 101.5 kcal mol^{-1}) C–H bonds are in line with those of alkane molecules (98.4 and 101.4 kcal mol^{-1} [69, 70]). The C–O bond connecting the hydroxyl function to the carbon chain shows a BDE of ≈ 94 kcal mol^{-1}. The weakest C–C bond is that connecting the secondary carbons at the α and β positions for *n*-propanol, *n*-butanol, *n*-pentanol

and *n*-hexanol. Its bond dissociation energy of approximately 86 kcal mol^{-1}, is about 1 – 1.5 kcal mol^{-1} lower than that of secondary carbons in alkanes (BDE = 87.5 kcal mol^{-1} [69, 70]).

Larger differences with the calculations of Oyeyemi [76, 77] are observed for secondary C–C bonds of the alkane-like moieties. Indeed, the average value of 89 kcal mol^{-1} from kinetic studies exceeds that by Oyeyemi by ≈ 2 kcal mol^{-1}. However, the selected value (i.e. 89 kcal/mol) is consistent with that proposed in the theoretical investigation of *n*-pentanol decomposition by Zhao et al. [78]. The same observations can be made for the terminal C–C bond, where a discrepancy of 1.5 kcal mol^{-1} is highlighted. ATcT estimates for *n*-propanol recommend a value of 87.3 kcal mol^{-1} for the terminal C–C bond, in agreement with the estimate from Pelucchi et al. [20]. ATcT values span the range of 87.5 – 89 kcal mol^{-1} [69, 70] in the parent alkane molecules moving from propane to pentane. Oyeyemi reports a value of 88.5 kcal mol^{-1}, while the average from kinetic studies is ≈ 90 kcal mol^{-1}, again in agreement with the investigation by Zhao et al. [78]. For the purposes of this study and considering the uncertainties in previous BDEs assessment, there exist clear indications of a negligible influence of the hydroxyl function beyond the β position.

Considering the above assumptions, the description of the kinetic rate constants will mostly focus on reaction pathways that are particular to alcohol oxidation, or those that largely differ from similar pathways in the parent alkanes. Aiming at the derivation of rate rules of general validity for *n*-C_3 – C_6 alcohols, *n*-butanol is taken as the model molecule for most of the discussion in the following Sections. By analogy with reaction classes typically considered to describe the pyrolysis and oxidation of *n*-alkanes [79-81], Sarathy et al. [5] reported an ensemble of 31 reaction classes to describe alcohol oxidation at high and low temperatures. Referring only to primary reactions of alcohols and to the successive reactivity of fuel radicals having the same carbon skeleton it is possible to condense the 31 reaction classes of Sarathy et al. [5] into 20 classes, as reported in Table 1.

Table 1: Reaction classes for alcohols pyrolysis and oxidation. Adapted from [5].

Reaction classes	
1. Unimolecular decompositions	11. $R\dot{O}_2$ isomerization reactions (RO_2=$\dot{Q}OOH$) including Waddington type reactions (RO_2=OH+CH_2O+C_{n-1} aldehyde)
2. Four-centered molecular decompositions	12. $\dot{Q}OOH$ decomposition to form $\dot{O}H$+alkenes/enols+carbonyl compounds

3.	H-atom abstractions	13.	$\dot{Q}OOH$ decomposition to form $H\dot{O}_2$+$C_n$enols
4.	Radical decomposition reactions	14.	$\dot{Q}OOH$ cyclization to form $\dot{O}H$ and epoxy (heterocyclic) alcohols
5.	Radical isomerization reactions	15.	Dehydration of $\dot{Q}OOH$ ($\dot{Q}OOH$ =H_2O+C_{n-1}aldehydes+$H\dot{C}O$)
6.	Reactions of O_2 with alcohols radicals to form $H\dot{O}_2$ and a C_n aldehyde/enol.	16.	Addition reactions of $\dot{Q}OOH$ to O_2 to form $\dot{O}_2QOOH$ (O_2+$\dot{Q}OOH$=$\dot{O}_2QOOH$) (including specific features of $\alpha\dot{Q}OOH$)
7.	Addition reactions of alcohol radicals to O_2 ($\dot{R}$ + O_2 = $R\dot{O}_2$)	17.	Isomerization reactions of $\dot{O}_2QOOH$ to form $\dot{O}H$ and carbonyl hydroxyalkyl hydroperoxides (CHHP).
8.	Recombination/disproportionation $\dot{R}'$+$R\dot{O}_2$=$R\dot{O}$+$R\dot{O}$ ($\dot{R}'$=$\dot{H}$, $\dot{C}H_3$, alcohol radicals)	18.	Decompositions of carbonyl hydroxyalkyl hydroperoxides (CHHP) to form $\dot{O}H$ and other carbonyl radical species
9.	Recombination/disproportionation $R'\dot{O}_2$+$R\dot{O}_2$=$R\dot{O}$+$R\dot{O}$ ($\dot{R}$=$\dot{H}$, $\dot{C}H_3$, alcohol radicals)	19.	Decompositions of carbonyl hydroxyalkyl hydroperoxides through the Korcek mechanism to form smaller organic acids and aldehydes
10.	$R\dot{O}_2$ concerted eliminations to form $H\dot{O}_2$ + aldehyde/enol	20.	H-atom abstraction reactions on carbonyl hydroxyalkyl hydroperoxides and decompositions

Contrary to Sarathy et al. [5], we neglect the discussion on successive decomposition or oxidation pathways of intermediate species such as unsaturated alcohols (enols), aldehydes and epoxy alcohols. The kinetic subsets for enols are adopted from previous developments [51-53] of the CRECK model attached. Rate coefficients for the *n*-hexenol isomers (unsaturated alcohols from *n*-hexanol oxidation) are based on analogy estimates from lower molecular weight enols (pentenol and butenol isomers). The kinetic subset for aldehydes pyrolysis and high and low temperature oxidation has been recently developed as discussed by Pelucchi et al. [21-23]. The consumption of intermediates such as epoxy alcohols (heterocyclic alcohols) via H-atom abstraction reactions is treated as described elsewhere [73]. The general kinetic scheme for pyrolysis and oxidation of alcohols is summarized in Figure 3. The kinetics adopted for the 20 reaction classes of Table 1 is described in details below.

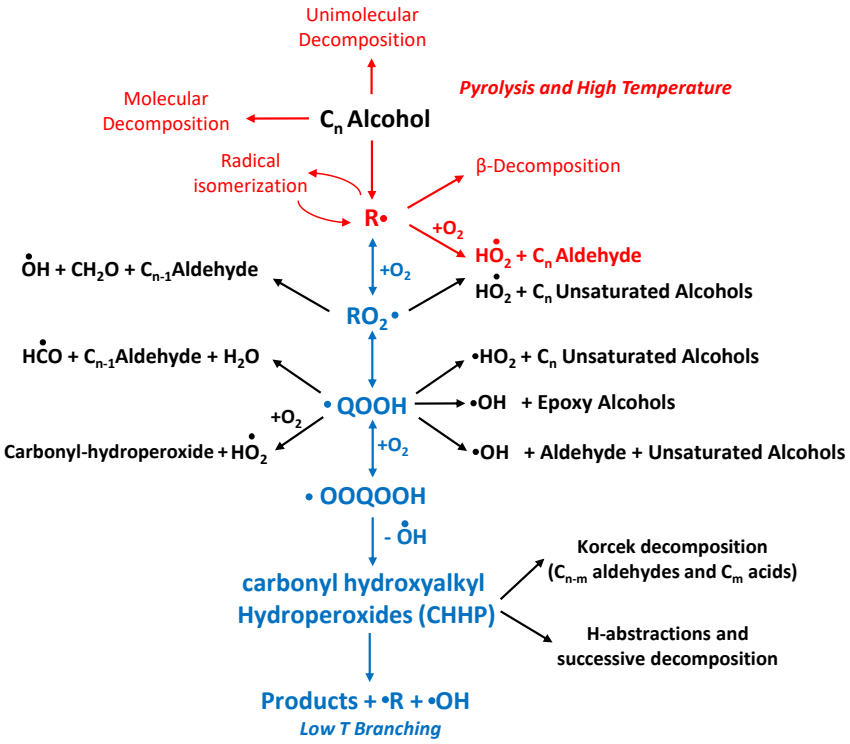

Figure 3: Simplified kinetic scheme for pyrolysis, high and low temperature oxidation of linear alcohols.

2.2 Unimolecular initiation reactions (Reaction Class 1)

Unimolecular initiation reactions involving a C–C, C–O, C–H or O–H bond fission are responsible for the initiation of the radical chain mechanism, in particular for pyrolysis and high temperature oxidation conditions. For this class of reaction the BDEs correspond to the activation energies of the elementary steps producing two radicals from the alcohol molecule. Indeed, the reverse radical-radical recombination reaction does not involve any energy barrier. From Figure 2 it is already possible to highlight the most favored initiation reactions, i.e. those involving the lower bond dissociation energy. The C_α–C_β bonds are the weakest, with activation energies in the order of ≈ 86 kcal mol^{-1}. The alcohol specific C–O bond connecting the carbon chain to the hydroxyl moiety (–OH) is the strongest, thus providing only a minor contribution to radical chain initiation. Figure 4 compares values from the literature [5, 78, 82, 83] with the rate constants adopted in this study for the unimolecular initiation reactions involving the fission of C–O (i.e. $C_n$alcohol = $\dot{O}H$ + $\dot{C}_n$ alkyl-radical), C_α–C_β (i.e. $C_n$alcohol = $\dot{C}H_2OH$ + $\dot{C}_{n-1}$ alkyl-radical) and C_β–C_γ (i.e. $C_n$alcohol = $\dot{C}_2H_4OH$ + $\dot{C}_{n-2}$ alkyl-radical), at p = 1 atm.

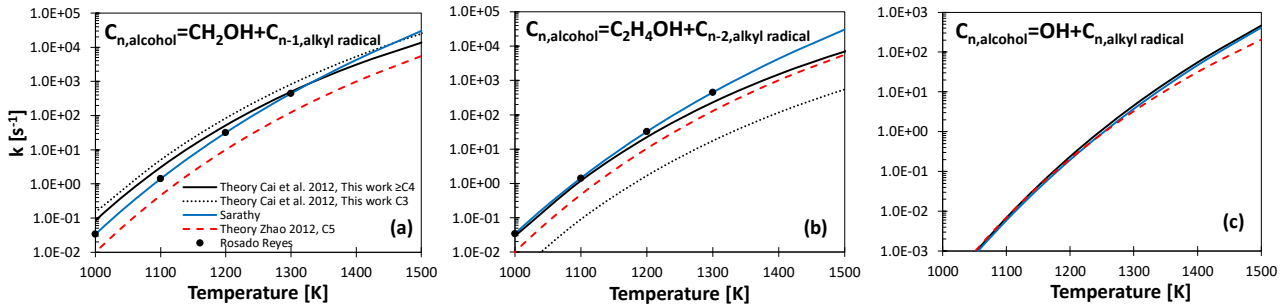

Figure 4: Comparison between unimolecular initiation rate constants involving the fission of C_α–O, C_α–C_β and C_β–C_γ bonds at p = 1 atm. Symbols: experimental data by Rosado-Reyes et al. [82]. Dotted black lines: Cai et al. [84] – this work (n-propanol), solid black lines: Cai et al. [83]- this work (≥ n-butanol), solid blue lines: Sarathy et al. [5] (n-butanol), dashed red lines: Zhao et al. [78] (n-pentanol).

Rosado-Reyes et al. [82] investigated experimentally the unimolecular decomposition of *n*-butanol in a single pulse shock tube (ST), at p ==1.5 – 6.2 bar and T = 1120 – 1250 K providing fits with an uncertainty of ≈ 3 kcal mol^{-1}, corresponding to a factor of ≈ 3 – 4 in the temperature range of the measurements. Zhao et al. [78] presented a theoretical investigation of *n*-pentanol decomposition at the CBS-QB3 level of theory. The variational implementation of the transition state theory (VTST) was applied to determine the high pressure limit rate constants for barrier-less reactions, and the pressure dependence determined with RRKM/master equation simulations. Rate constants were provided for the temperature range T = 800 – 2000 K. Similarly, Cai et al. [83, 84] calculated pressure and temperature dependent rate constants for a series of butanol isomers, including *n*-butanol (1-butanol) and 2-butanol, at the CBS-APNO level of theory. According to the authors, inaccuracies as large as a factor of ≈ 2 – 3 are expected from the theoretical methods applied.

As in the kinetic model of Li et al. [54], for the C_α–C_β decomposition channel (Figure 4a) in *n*-propanol we adopt the rate constants for 2-butanol = $\dot{C}_2H_5$ + $CH_3\dot{C}HOH$ calculated by Cai et al. [84], based on similarities between bond dissociation energies as discussed by Man et al. [75]. The same analogy applies to the decomposition reactions involving C_β–C_γ (Figure 4b), for which we adopted the analogous rate constant for 2-butanol = $\dot{C}H_3$ + $\dot{C}H_2CH(OH)CH_3$. This choice was made based on improved agreement obtained with pyrolysis experiments discussed in Section 4 and in Part II.

For higher molecular weight alcohols ($C_n \geq 4$) we adopt the whole set of rate constants calculated by Cai et al. [83] for *n*-butanol. Concerning the C–O bond breaking channel (C_n alcohols = $\dot{O}H$ + $\dot{C}_n$ alkyl-radical, Figure 4c), we adopt the values proposed by Li et al. [54] which is in line with that suggested by Zhao et al.

[78]. No determination of this decomposition pathways were in fact provided in the experimental [82] and theoretical studies [83, 84] mentioned above.

In general, the set of values selected in the present work agrees with Rosado-Reyes et al. [82] within the reported uncertainties. Larger deviations, up to a factor of ≈ 5, are highlighted for the dominating C_α–C_β channel with respect to the determination of Zhao et al. [78] for *n*-pentanol.

Figure 5(a) shows the total decomposition rate constants for *n*-C_3 – C_6 alcohols obtained as the sum of the unimolecular decomposition channels involving C–C and C–O bonds fission. Aiming to highlight inconsistencies still existing in the literature on alcohols pyrolysis and combustion, it should be observed that n-propanol shows a total rate of decomposition ≈ 20% higher than that of *n*-butanol, in disagreement with the expected increase of total decomposition rates from bond fission reactions with increasing carbon chain length. Figure 5(b) compares the relative importance of the different unimolecular decomposition channels, highlighting its correlation with bond dissociation energies (C–OH, ≈ 94 kcal mol^{-1} < Cs–Cp, ≈ 89 kcal mol^{-1} < Cs–Cs, ≈ 88 kcal mol^{-1} < C_α–C_β, ≈ 86 kcal mol^{-1}). The decomposition reactions $C_n$alcohol = $\dot{C}H_2OH$ + $\dot{C}_{n-1}$ alkyl-radical play the major role, covering from ≈ 97% in *n*-propanol to ≈ 43% in *n*-hexanol. Despite the selected rate parameters showing good agreement with the pyrolysis experiments, it is worth underlining the need of a systematic theoretical investigation of unimolecular initiation reactions to reconcile the inconsistent information available in the literature.

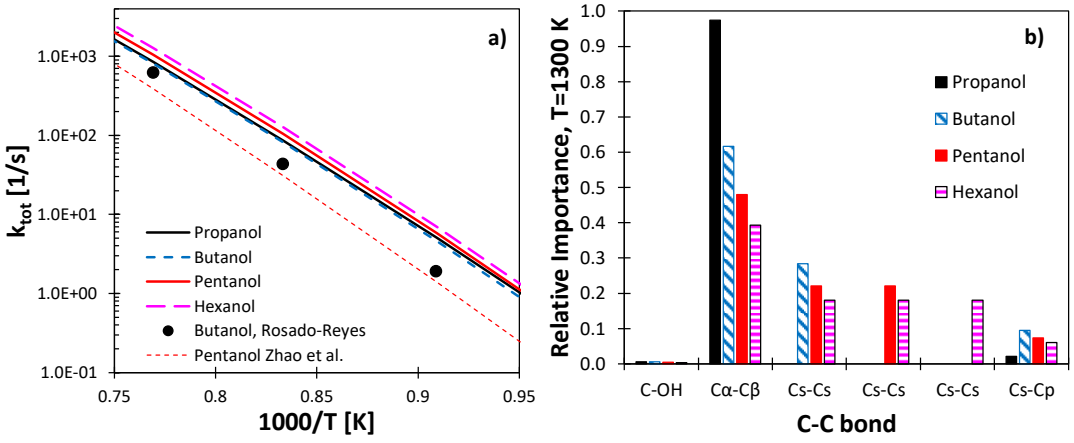

Figure 5: a) Total decomposition rate constant for n-C_3 – C_6 alcohols obtained from the rate constant values adopted in this work compared with literature values [78, 82]. b) Relative importance of the different unimolecular decomposition channels.

Reaction pathways involving the breaking of a C–H or O–H bonds generally provide a negligible contribution to the unimolecular decomposition of the fuel molecule. The same reference kinetic parameter is adopted for the reverse recombination reaction (k = 5.0 × 10^{13} cm^3 mol^{-1} s^{-1}). Rate parameters for these reactions in the reverse decomposition direction are consistent with the bond dissociation energies of C–H and O–H bonds discussed at the beginning of Section 2.

2.3 Four-centered molecular decomposition reactions: dehydration and dehydrogenation (Reaction Class 2)

This class of reactions proceeds through a four-center cyclic transition state, forming the parent alkenes and H_2O. Figure 6(a) compares the rate constants adopted in this work at p = 1 atm with the values proposed in previous studies [5, 78, 82, 83]. The proposed values agree within a factor of two with the values proposed by Sarathy et al. [5], Cai et al. [83] and Rosado-Reyes et al. [82]. The rate constant from Zhao et al. [78] is approximately six times lower.

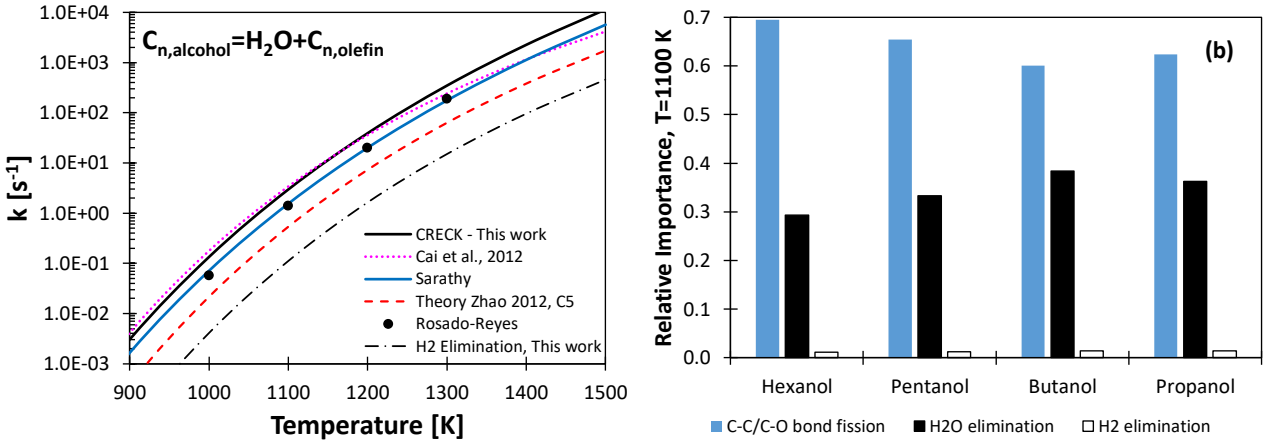

Figure 6: a) Comparison between rate constants for four-centered molecular dehydration reaction from different sources [5, 78, 82, 83]. b) Relative contribution of four centered molecular reactions to the total unimolecular decomposition rate of n-C_3 – C_6 alcohols.

Four-centered molecular dehydrogenation producing the parent aldehyde can also occur as discussed in Grana et al. [52] and Nativel et al. [53] for *n*-butanol and *n*-pentanol, respectively. Rate constants are adopted based on the analogy with the same reaction in *n*-alkanes [85] and their contribution is much lower (≈ 30 times) compared to dehydration.

Figure 6(b) shows the relative contributions of four-centered molecular reactions and bond fission reactions to the unimolecular decomposition of *n*-C_3-C_6 alcohols at $T = 1100$ K and $p = 1$ atm, confirming the negligible role of the dehydrogenation channel. The dehydration reaction, for which we adopted the same rate parameters for the full series of alcohols because the reactions proceed through analogous four-centered transition states, contributes approximately 30 – 40% to the total decomposition rate constant. As expected the relative weight decreases for increasing molecular weight, with the exception of *n*-propanol. This deviation is related to the different set of unimolecular decomposition reactions adopted for n-propanol, as discussed in Section 2.2.

2.4 H-atom abstraction reactions (Reaction Class 3)

Rate parameters of H-atom abstraction reactions are determined according to the systematic approach described by Ranzi et al. [86]. Regarding the alkane-like moiety of *n*-C_3-C_6 alcohols, primary and secondary sites are treated according to alkane rules for analogous H-atom abstraction sites in the general form of Ṙ + R'H = RH + Ṙ', where R'H is a fuel molecule and Ṙ is a generic abstracting radical. To account for the stronger BDE for the C_β–H bond, the reference values adopted for alkane-like secondary sites have been decreased by 25%. Kinetic parameters for the weakened secondary C_α–H bond have been obtained by increasing the reference rate constants by 75%. As from the following discussions, such modifications are well within the expected uncertainty of theoretical and experimental determinations available for the most important abstracting radicals: Ḣ, ȮH, $HȮ_2$, $ĊH_3$. The same reference parameters have been applied to the entire alcohol series. Such reference parameters are reported as Supplementary Material (Table S3).

Figure 7 compares the total rate constants of H-atom abstraction from *n*-butanol by Ḣ, ȮH, $HȮ_2$ and $ĊH_3$ implemented in the kinetic model attached to this work with those from previous theoretical [41-43], experimental [44, 45, 48, 49, 87] and kinetic modeling studies [5, 83]. Regarding H-atom abstraction by Ḣ atoms, our total rate constant agrees with the experimental determination by Oganesyan et al. [87] and with Cai et al. [83] within a factor of ≈ 2. Sarathy et al. [5] propose a value that is approximately three times higher than the estimate by Cai et al. [83]. In terms of selectivity to the available H-atom abstraction sites (O, α, β, secondary and primary) at $T = 1300$ K, trends are as expected from the BDEs (Figure 2) and from the number

of available hydrogen atoms. Abstraction from the α-site is the most favored channel, followed by the secondary position of the alkane-like moiety, β, the terminal primary position and the H-atom abstraction from the hydroxyl substitution. The selectivities from the kinetic model attached to this study are 46%, 25%, 15%, 9% and 5%. Zhou et al. [43] presented the only theoretical determination of H-atom abstraction reactions by ȮH from *n*-butanol over the entire temperature range of interest for pyrolysis and combustion applications ($T = 500 - 2000$ K). The total rate constant by Zhou et al. agrees with the higher temperature (T > 900 K) experimental determinations [45, 49] within a factor of 1.5, while larger deviations exist in comparison with lower temperature data [44, 48]. Our proposed rate constant agrees with the experimental data and with the values adopted in [5, 83] within a factor of ≈ 2. The calculations by Zhou et al. [43] show an unexpected dominant role of the H-atom abstraction from the β position, in evident disagreement with previously validated kinetic models. Better agreement in terms of relative selectivities at $T = 800$ K is observed between our set of rate constants and those adopted in [5, 83]. In particular the dominating channel is once again α (40%), followed by the alkane-like secondary position (25%), β (17%), primary site (13%) and the hydroxyl moiety (5%).

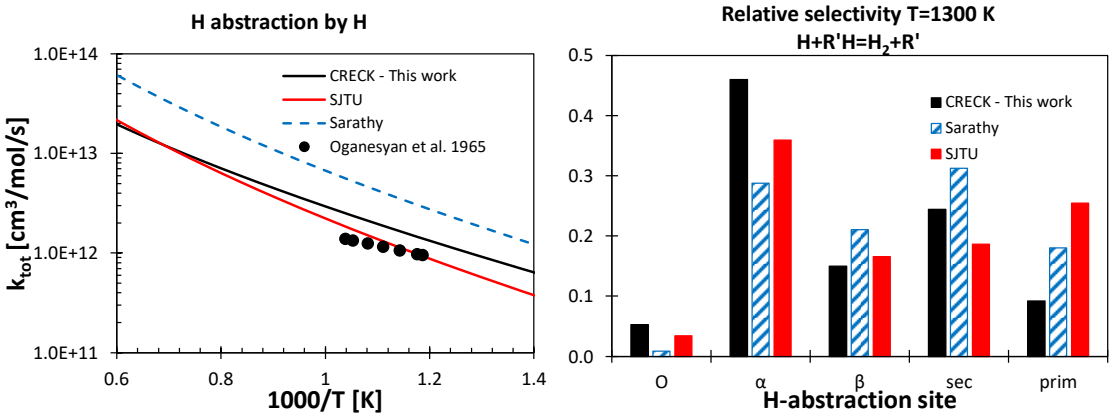

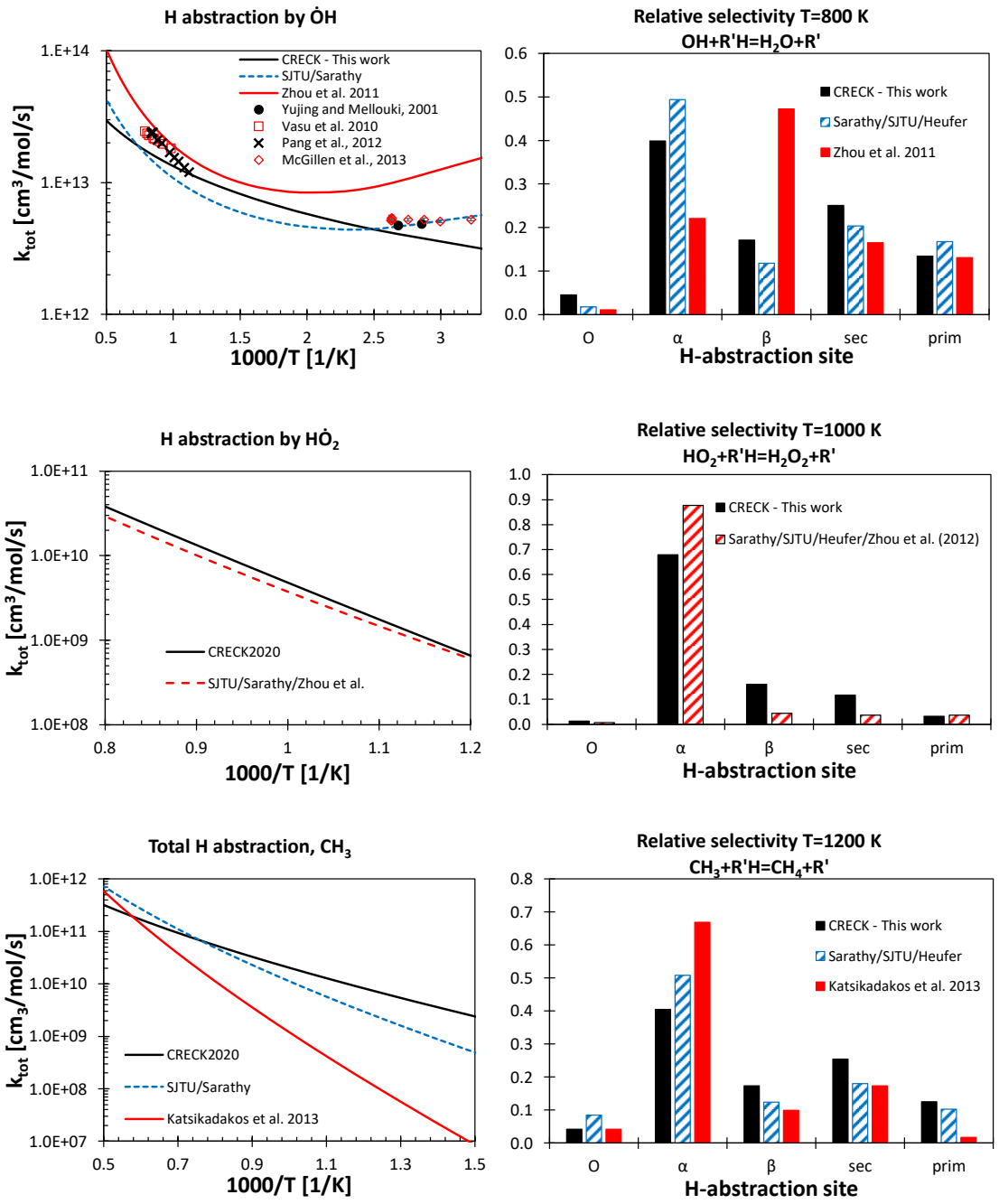

Figure 7. Left: total rate constants of H-atom abstraction reactions by Ḣ, ȮH, HȮ₂ and ĊH₃ on n-butanol from this work (black) and from the literature [5, 41-45, 48, 49, 83, 87]; right: relative selectivity to the different H-atom abstraction site for n-butanol from this work (black) and from the literature.

The rate constant of H-atom abstraction by HȮ₂ adopted in our work agrees within 20% with the calculations of Zhou et al. [41] in terms of absolute rate. This agreement was obtained by modifying the reference kinetic parameters discussed at the beginning of this Section, through a global increase of a factor of 8.4. The *n*-butanol models of Sarathy et al. [5] and Cai et al. [83] adopt the theoretical values of Zhou et al. [41] for the single channels. In terms of relative importance, this set of rate constants results in a very high

selectivity (i.e. 88% at T = 1000 K) in favor of the α site. According to our systematic analysis presented here and to previous modeling efforts [20, 51-53, 56] a more realistic selectivity (O = 1%, α = 68%, β = 16%, secondary = 12%, primary = 3%) was obtained distributing the increase of the absolute rate (i.e. a factor of 8.4) by multiplying the reference parameters by 3.5 for α, 2 for β and 1.2 for the hydroxyl moiety. In fact, the impact of the high selectivity towards the α position proposed by Zhou et al. [41] would significantly worsen model predictions.

Katsikadakos et al. [42] calculated rate constants for the H-atom abstraction reactions by methyl radical ($\dot{C}H_3$) from *n*-butanol. Reasonable agreement, i.e. < factor of 3, with our rate constants and those from Sarathy et al. [5] and Cai et al. [83] is observed only for T > 1350 K. At lower temperatures deviations as large as three orders of magnitude are highlighted. Taking advantage of a quite significant number of pyrolysis data [37, 54, 55, 59, 84] where the H-atom abstractions by $\dot{C}H_3$ play a significant role for the validation of our model, we observed negative effects on model performances when implementing the theoretical values. Moreover, our reference kinetic parameters were found to agree quite satisfactorily (< factor of 3) with the estimates reported in [5, 83], both in terms of absolute rate constant and relative selectivities, as reported in Figure 7. Also for H-atom abstraction by methyl radical the dominating channel is once again α (40%), followed by the alkane-like secondary position (25%), the secondary β site (17%), the terminal primary site (13%) and the hydroxyl moiety (5%).

2.5 Decomposition and isomerization reactions of alcohols radicals. (Reaction Classes 4 and 5)

At high temperatures (e.g. T > 900 K) fuel radicals can decompose via β-scission reactions, or isomerize through internal hydrogen abstractions proceeding through a cyclic transition state.

Table 2 shows the reference rate parameters adopted in the kinetic model discussed here, taking *n*-butanol as an example. The selected values were adopted from our previous kinetics studies [51-53] with some minor adjustment based on our literature review and on the comprehensive model validation summarized in Section 4 and discussed in Part II of this study [56]. The same rate rules are systematically

applied to the entire *n*-$C_3 - C_6$ alcohol series. The rate constants are compared with those proposed in the review by Sarathy et al. [5] in Figure S1 of the Supplementary material.

Alkoxy radicals ($R_nȮ$) mostly decompose producing formaldehyde (CH_2O) and a $Ċ_{n-1}$ primary radical (e.g. *n*-propyl radical). Alkoxy radicals are in general very reactive compared to primary and secondary alkyl radicals, as expected from the high BDE of the O–H bond. As a result, the decomposition of alkoxy radicals (RȮ) are about an order of magnitude faster compared to the β-decomposition of the other alkyl radicals described in the following. An additional pathway leads to the fission of the $C_α$–H bond located at the β position to the unpaired electron producing Ḣ atoms and the parent C_n aldehyde (e.g. *n*-butanal). Compared to similar reactions in alkanes, this latter step is particularly favored for alcohols due to the lower BDE of $C_α$–H, but is still of much lower importance compared to β-scissions involving a C–C bond.

The secondary radical Ṙα largely decomposes forming ethenol (C_2H_3OH) and a $Ċ_{n-2}$ primary radical (e.g. ethyl radical). The rate constant for this reaction is over an order of magnitude higher than the two other possible β-scission reactions involving the breaking of a C–H bond, forming a C_n unsaturated alcohol (*n*-butenol) or of an O–H bond. This latter pathway leads to the formation of the parent C_n aldehyde.

The decomposition of the secondary radical in the β position primarily leads to the formation of the parent C_n 1-olefin by C–O bond cleavage, thus releasing ȮH radicals. An additional important decomposition route is in the formation of 2-propenol (C_3H_5OH) and a $Ċ_{n-3}$ alkyl radical (e.g. methyl radical). Another available minor pathways produce Ḣ atoms and C_n enols or aldehydes. Aiming for a compact subset of reactions to describe alcohols pyrolysis and oxidation we only consider one representative lumped C_n enol formed from the decomposition of *n*-$C_3 - C_6$ alcohols radicals.

Table 2: Rate coefficients for alcohol radical isomerization and decomposition reactions. The same rate rules are adopted to describe the decomposition of radicals for the series nC_3-C_6 alcohols. Modifications to the pre-exponential factors (A) or to the activation energies (Ea) with respect to Grana et al. [52] are provided. Notes: a) for improved agreement in speciation data prediction at high temperatures for CH_2O and C_n aldehyde, b) for better agreement with rate constant suggestion from Sarathy et al. [5], c) for better agreement with theoretical determination by Zhang et al. [88].

	n-butanol radicals	A [s^{-1}]	n	Ea [cal mol^{-1}]	Ref.	Notes
$R_nȮ$	**↔ CH_2O + $Ċ_{n-1}$ Alkyl Radical**	6.0×10^{13}	0.00	15000.	[52]	A/0.5[a]

	↔ **Ḣ + C_n Aldehyde**	1.0×10^{13}	0.00	26000.	[52]	A/3[a]
$\dot{R}_n\alpha$	↔ **Ḣ + C_n Aldehyde**	3.0×10^{13}	0.00	38000.	[52]	Ea=+1 kcal/mol[b]
	↔ **C_2H_3OH + $\dot{C}_{n-2}$ Alkyl Radical**	1.0×10^{13}	0.00	28000.	[52]	
	↔ **Ḣ + C_n Enol**	1.0×10^{13}	0.00	38000.	[52]	
$\dot{R}_n\beta$	↔ **ȮH + C_n Alkene**	7.2×10^{42}	-9.04	37600.	[83]	
	↔ **C_3H_5OH + $\dot{C}_{n-3}$ Alkyl Radical**	5.0×10^{12}	0.00	27000.	[83]	
	↔ **Ḣ + C_n Enol**	1.0×10^{13}	0.00	34000.	[52]	
	↔ **Ḣ + C_n Aldehyde**	3.0×10^{13}	0.00	38000.	[52]	Ea=+1 kcal/mol[b]
	↔ ***RȮ (4 member ring)***	5.0×10^{11}	0.00	26000.	[52]	
$\dot{R}_n$sec	↔ **CH_2OH + C_{n-1} Alkene**	6.0×10^{13}	0.00	31000.	[52]	A/0.5, Ea=+1 kcal/mol[c]
	↔ **Ḣ + C_n Enol**	3.0×10^{13}	0.00	38000.	[52]	Ea=+1 kcal/mol[b]
	↔ ***RȮ (5 member ring)***	1.0×10^{11}	0.00	23000.	[52]	
	↔ **C_2H_4 + $\dot{C}H_2(CH_2)_{n-3}OH$**	3.0×10^{13}	0.00	30000.	[52]	
$\dot{R}_n$prim	↔ **Ḣ + C_n Enol**	2.0×10^{13}	0.00	37000.	[52]	A/1.5, Ea=+1 kcal/mol[b]
	↔ ***RȮ (6 member ring)***	1.6×10^{10}	0.00	16000.	[52]	
	↔ ***Ṙα (5 member ring)***	2.0×10^{11}	0.00	19600.	[52]	

Secondary radicals of the alkane-like moiety mainly decompose forming hydroxymethylene radical ($\dot{C}H_2OH$) and a C_{n-1} alkene (e.g. propene). For alcohols heavier than *n*-butanol, an additional pathway forming 3-butenol (C_4H_7OH) and a $\dot{C}_{n-4}$ alkyl radical is available. Rate constants for this latter channel are estimated by analogy with β-scission reactions of secondary alkyl radicals [74]. Primary radicals largely decompose to form ethylene (C_2H_4) and the primary radical of a $\dot{C}_{n-2}$ alcohol (e.g. $\dot{C}_2H_4OH$). Even for these last cases the dehydrogenation channels are less favored at the conditions of interest ($T = 500 - 2000$ K).

Isomerization reactions of alcohols radicals are explained on the basis of internal H-atom abstraction reactions, via 5-membered, 6-membered and 7-memebered ring intermediates. The rate constants of these isomerization reactions are estimated in terms of the number of atoms in the transition state ring structure (including the H atom) and the type of sites involved in the H-atom transfer [89]. To this aim, the rates are also influenced by the different bond dissociation energies of the alcohol-specific moiety and need to be

accounted for as discussed in Nativel et al. [53]. For this reason we also consider 4-membered transition state structures leading to the internal H-atom abstraction of the hydrogen of the weakest C_α–H bond.

2.6 Reactions of O_2 with alcohols radicals to form $H\dot{O}_2$ and a C_n aldehyde/enol (Reaction Class 6).

Stable C_n aldehydes and enols are formed at high temperatures through β-scission reactions involving the C–H bond. At lower temperatures the same compounds can be formed by direct H-atom abstraction by O_2 forming an unsaturated bond and $H\dot{O}_2$ ($\dot{R}_n + O_2 = H\dot{O}_2 + R_n$-aldehyde/enol). In particular, the reactions of primary and secondary radicals of the alkane-like moiety and of the secondary radicals in the β position form the parent unsaturated alcohol. Rate constants for this reaction class have been adopted from similar reactions of alkane fuel combustion ($k = 3 \times 10^{11}$ exp(–3500 [cal/mol]/RT) [cm^3/mol/s]). Reactions of α radicals with O_2 produce the parent aldehyde and $H\dot{O}_2$. Due to the high selectivity towards the formation of α radicals through H-atom abstraction reactions (Section 2.3), this latter pathway has a high impact on alcohols reactivity and largely justifies, from a purely chemical kinetic perspective, the high octane rating of alcohol fuels. Indeed, only radicals in the β position and in the alkane-like moiety effectively undergo addition to O_2, forming the peroxy radical and activating the branching pathways responsible for low temperature reactivity. Despite a more systematic theoretical evaluation of $\dot{R}\alpha + O_2$ for a series of alcohols would be necessary in order to obtain more accurate rate rules, the high pressure limit rate constant computed by Zádor et al. [38] has been adopted for $\dot{R}_n\alpha + O_2 = H\dot{O}_2 + C_n$ aldehyde. According to Zádor et al. [38], the concerted elimination reaction yielding aldehyde and $H\dot{O}_2$ proceeds through the formation of an aldehyde-HO_2 complex, rapidly decomposing to the products.

2.7 Addition reactions of alcohol radicals to O_2 ($\dot{R} + O_2 = R\dot{O}_2$) (Reaction Class 7)

Similarly to alkanes, the transition between high and low temperature regimes depends on the competition between β-scission reactions of alcohol radicals (Section 2.4) and their addition to O_2, forming hydroxyalkyl-peroxy radicals ($R\dot{O}_2$). Although this step does not directly determine the rate of chain branching, the correct description of the relative concentrations of alkyl and peroxyl radicals is a necessary condition to fully characterize low temperature ignition phenomena. As reviewed by Sarathy et al. [5] no specific theoretical studies have been dedicated to a comprehensive assessment of alcohols specific rate constants for this reaction class, therefore we base our reference rate parameters for alcohol fuels on the rate rules provided by Ranzi et al. [90] for alkanes. In particular we adopt a value of 1.0×10^{12} cm^3 mol^{-1} s^{-1} for the primary radicals and a value of 2.0×10^{12} cm^3 mol^{-1} s^{-1} for secondary radicals, including β (Table 3). We assume that $\dot{R}_n\alpha$ radical does not undergo addition to O_2. Indeed, as reported in the theoretical studies for ethanol by Zádor et al. [38] and da Silva et al. [31, 32], at the conditions of interest for combustion applications, the peroxy radical obtained from such an addition reaction would rapidly dissociate back to the reactant, favoring the direct pathway to $H\dot{O}_2$ and the parent aldehyde.

2.8 Recombination/Disproportionation reactions of $R\dot{O}_2$ radicals: $R\dot{O}_2 + R'\dot{O}_2$ and $\dot{R} + R'\dot{O}_2$ ($\dot{R}'$ = $\dot{H}$, $\dot{C}H_3$, alcohol radicals) (Reaction Classes 8 and 9)

$R\dot{O}_2$ radicals can undergo recombination/disproportionation reactions forming $R\dot{O}$ and $R'\dot{O}$ radicals. The recombination of hydroxyalkyl-peroxy radicals ($R\dot{O}_2 + R'\dot{O}_2$) produces O_2 and a ROOR' intermediate that rapidly decomposes to two alkoxy radical $R\dot{O}$ and $R'\dot{O}$, whose decomposition rate is also very fast, by analogy with the $R\dot{O}$ radicals decomposition described in Section 2.4. Depending on the chain length of the fuel (C_nOH) on the nature of $\dot{R}'$ ($\dot{H}$, $\dot{C}H_3$, alcohol radicals) and on the location of the peroxy radical moiety, $R\dot{O}$ and $R'\dot{O}$ decomposition products are C_m aldehydes of different molecular weight (m < n, formaldehyde, acetaldehyde, propanal, butanal, etc.), primary alkyl radicals of smaller alcohols ($\dot{C}H_2OH$, $\dot{C}H_2CH_2OH$, $\dot{C}H_2CH_2CH_2OH$, etc.), $\dot{O}H$ and $CH_3\dot{O}$. The recombination of fuel radicals $\dot{R}$ and $R'\dot{O}_2$ produces the same $R\dot{O}$ and $R'\dot{O}$ from the decomposition of the ROOR' intermediate. Also in this case $R\dot{O}$ and $R'\dot{O}$ are assumed to directly decompose

to the same products. Similar reactions for *n*-alkanes have been thoroughly discussed recently by Ranzi and co-workers [73], from which we adopt the reference kinetic parameters (Table 3).

2.9 $R\dot{O}_2$ concerted eliminations to form $H\dot{O}_2$ + aldehyde/enol (Reaction Class 10)

$R\dot{O}_2$ radicals can eliminate $H\dot{O}_2$ forming a C_n aldehyde or enol. The same reaction class produces $H\dot{O}_2$ and alkenes in *n*-alkanes low temperature oxidation. Reference rate parameters have been adopted from the review paper of Sarathy et al. [5]. From a low temperature reactivity stand point this reaction directly competes with the isomerization of $R\dot{O}_2$ radicals described in the following Section.

2.10 $R\dot{O}_2$ isomerization reactions ($R\dot{O}_2 \rightleftharpoons \dot{Q}OOH$) including Waddington type reactions ($R\dot{O}_2 = \dot{O}H + CH_2O + C_{n-1}$ aldehyde) (Reaction Class 11)

Intra-molecular H-atom abstraction reaction of hydroxyalkyl-peroxy radicals ($R\dot{O}_2$) to form hydroperoxyl-alkylhydroxy radicals ($\dot{Q}OOH$) are the second step in the low temperature chain branching pathway of alcohols oxidation (Figure 2). 5- and 6- membered isomerization reactions by tying up 3 and 4 internal rotors respectively are considered herein. As discussed previously [73, 74, 79, 90, 91], the activation energy can be computed as $E_a = E^0_{ref,R} + EC_{R'H} + E_{rs}$, where $E^0_{ref,R}$ is the reference activation energy for a peroxyl radical abstracting a primary H-atom (21.5 kcal mol^{-1}) [86], $EC_{R'H}$ is the correction to account for the type of H-atom abstracted based on the bond dissociation energies discussed in Section 2 (i.e., in kcal mol^{-1}, 0.0 - primary, -2.5 – secondary, –4.0 - α, +1.0 - β, +2 - OH) and E_{rs} is the ring strain energy (i.e., in kcal mol^{-1}, +1.0 - 6–membered, +7.0 - 5–membered). As an example, for the isomerization reaction reported in Figure 8 the activation energy is 18.5 kcal mol^{-1} in the forward direction.

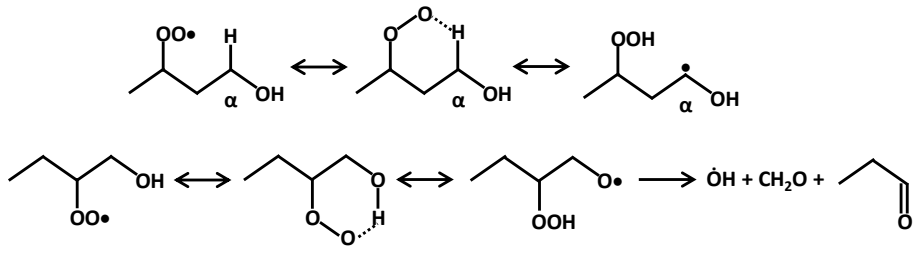

Figure 8: example 6-membered isomerization reactions in n-butanol oxidation. Top: sec-RȮ$_2$ producing α-ȽOOH, bottom (Waddington mechanism): β-RȮ$_2$ producing an hydroperoxy alkoxyradical and its successive decomposition.

The reference frequency factor is 2.0×10^{11} s^{-1} derived from the reference frequency factor for the internal H-atom abstraction of one single primary hydrogen atom through a 6-membered transition state. Lowering the number of hindered internal rotors by one (e.g. in the case of a 5-membered isomerization) increases the frequency factor by $10^{0.8}$ s^{-1}, resulting in a reference pre-exponential factor of $10^{11.8}$ s^{-1}, and increases the activation energy by 6 kcal mol^{-1}. Reverse rate constants can also be estimated in a similar fashion as discussed in previous studies [73, 74, 79, 90, 91], again, taking into account the relative stability of ȽOOH radicals as retrieved from the bond dissociation energies (i.e. α-ȽOOH > sec-ȽOOH > β-ȽOOH > prim-ȽOOH) of Section 2. Reference rate parameters for the RȮ$_2$ ⇌ ȽOOH isomerization reactions are reported in Table 3.

β-RȮ$_2$ radicals (C_n) can isomerize to transfer the H-atom of the hydroxyl moiety to form alkoxy hydroperoxy radicals, that rapidly decompose to form formaldehyde, C_{n-1} aldehyde and ȮH (RȮ$_2$ = ȮH + CH_2O + C_{n-1} aldehyde). This specific reaction is known as the Waddington-mechanism [92]. The associated reference rate parameters adopted from Sarathy et al. [5] in our previous kinetic modeling studies of alcohol low temperature oxidation [17, 20] have been corrected according to the recent theoretical study by Li et al. [93]. The reference kinetic parameters were increased by a factor of 6 (Table 3), agreeing within a factor of two with the recent theoretical calculation.

2.11 ȽOOH radical decomposition reactions (Reaction Classes 12 to 15)

The low temperature branching pathway can be inhibited by the occurrence of unimolecular decomposition reactions of ȽOOH radicals. If the radical site is located γ to the hydroperoxy function (–OOH)

β-scission reactions forming an alkene (or an enol) and a carbonyl compound (aldehydes, hydroxyl aldehydes), together with ȮH radical occur. Q̇OOH radicals with the radical site located β to the OOH group decompose to form HȮ$_2$ and a C$_n$ enol. Reference rate parameters are taken based on the analogy with *n*-alkanes [73, 74, 79, 90, 91] (Table 3). By analogy to cyclic ether formation in the oxidation of alkanes, cyclization reactions produce epoxy alcohols and an ȮH radical. Once again the energy barrier and the frequency factor depend on the size of the cyclic species formed. Specifically, an activation energy of 18 kcal mol^{-1} is assumed for the formation of oxirane alcohols (3-membered cyclic ether moiety), this decreases to 17 kcal mol^{-1} for oxetane alcohols (4-membered cyclic ether moiety) and to 8.5 kcal mol^{-1} for epoxy alcohols with a 5-membered cyclic ether moiety. The frequency factor ranges from 10^{12} s^{-1} to $10^{10.4}$ s^{-1}, depending on the number of rotors tied up. H-atom abstraction reactions are considered so as to take into account the consumption of epoxy alcohols. Rate constants are based on analogy with H-atom abstraction reactions on cyclic ethers in alkanes [73, 74, 79, 90, 91].

In addition to alkane-like decomposition reactions, Welz et al. [40] proposed and investigated an unconventional dehydration pathway of α-Q̇OOH radicals occurring in alcohols oxidation (Figure 9). The rate constant is estimated in this work taking into account the formation of a cyclic transition state and the calculated energy barrier (≈ 13 kcal mol^{-1}). In addition to water these reactions produce a C$_{n-1}$ aldehyde and formyl radical (HĊO).

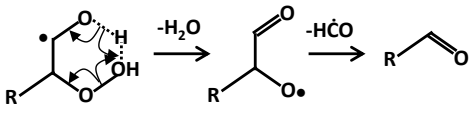

Figure 9: Dehydration channel of Q̇OOH radicals [40] and successive decomposition.

2.12 Q̇OOH radicals addition to O$_2$ (Q̇OOH + O$_2$ = Ȯ$_2$QOOH) (Reaction Class 16)

The third step in the low temperature chain branching pathway involves a second addition to O$_2$ to form Ȯ$_2$QOOH radicals. Rate constants are taken in analogy with the first addition Ṙ + O$_2$ = RȮ$_2$ and depend on the nature of the radical site. If the radical site is located in α (α-hydroxy-hydroperoxyalkyl radical) its interaction with O$_2$ directly leads to the formation of a carbonyl-hydroperoxide (e.g. hydroperoxy butanal)

and $H\dot{O}_2$. An example of this peculiar reaction is represented in Figure 10. Rate constants are taken in analogy with the $\dot{R}_\alpha + O_2$ reaction (Reaction class 6) investigated by Zádor et al. [38]. The consumption pathways of the carbonyl-hydroperoxide species thus obtained are already described in the subset of the CRECK model describing the consumption of ketohydroperoxides formed in *n*-alkane oxidation (e.g. *n*-butane).

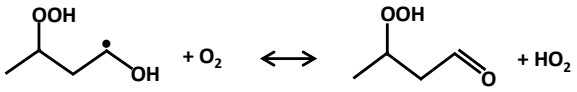

Figure 10: α-hydroxy-hydroperoxyalkyl radical and its interactions with O_2 to form a carbonyl-hydroperoxide (e.g. hydroperoxy butanal) and $H\dot{O}_2$.

2.13 Isomerization reactions of $\dot{O}_2$QOOH to form ȮH and a carbonyl hydroxyalkyl hydroperoxide (Reaction Class 17)

The same rate rules described for the first isomerization ($R\dot{O}_2 \rightleftharpoons \dot{Q}OOH$, reaction class 11) are adopted to describe the second isomerization leading to the formation of ȮH and a carbonyl alkyl hydroperoxide and ȮH. As in the description of alkanes low temperature branching pathways in the CRECK kinetic model, these reactions are considered in the lumped form directly eliminating ȮH, neglecting the formation of the intermediate that is rapidly decomposed (Figure 11).

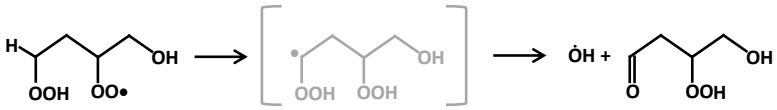

Figure 11: example of a 6-membered second isomerization reaction directly forming OH and a carbonyl alkyl hydroperoxide. The intermediate species in grey is neglected in the kinetic model.

2.14 Decomposition of carbonyl hydroxyalkyl hydroperoxides to form oxygenated radical species, ȮH and and carbonyl compounds (Reaction Class 18)

The last step of the low temperature branching pathway leads to the formation of oxygenated radical species and stable molecules, together with an ȮH radical. The rate limiting event in this decomposition reaction is the fission of the O–OH bond of the hydroperoxyl functional group, successive β-scission reactions are responsible for the formation of the oxygenated products. Reference rate parameters are reported in

Table 3. Figure 12 shows an example of n-butanol carbonyl hydroxyalkyl hydroperoxides (CHHP) decomposition reactions.

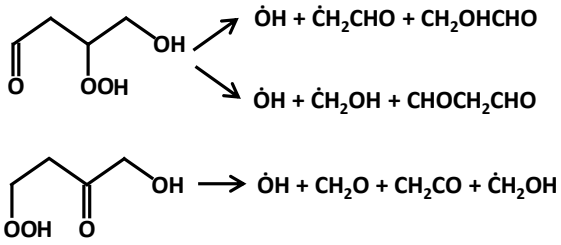

Figure 12: Example of CHHP branching decomposition reactions.

2.15 Decomposition of carbonyl hydroxyalkyl hydroperoxides through the Korcek mechanism and H-atom abstraction reactions

Ranzi et al. [73] recently proposed additional consumption pathways for ketohydroperoxides in *n*-alkanes, that directly compete with the branching decomposition of ketohydroperoxides at very low temperatures and relatively high fuel concentration, inhibiting reactivity. For completeness, the same alternative channels are considered herein for the decomposition of carbonyl alkyl hydroperoxides, despite their negligible impact on overall low temperature reactivity for the available targets (Section 4 and Part II [56]).

Korcek type mechanisms produce aldehydes or carbonyl compounds and organic acids (e.g. formic and acetic acids) (Figure 13), while H-atom abstraction reactions and successive β-scissions produce hydroxyl diones. Successive reactions of formic and acetic acids are already described in the core chemistry of the CRECK kinetic model. For simplicity and due to the lack of experimental evidences on the formation of such species (i.e. hydroxyl diones) we consider them as directly decomposed to stable molecules so as to respect the atomic balance.

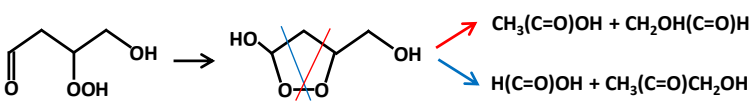

Figure 13: Example of Korcek mechanism decomposition of CHHP in n-butanol oxidation.

To conclude Section 3, Table 3 provides a synoptic view of reference kinetic parameters to describe the low temperature oxidation of alcohols.

*Table 3: Reference kinetic parameters for the low temperature oxidation of alcohols. Units are cal, cm^3, mol, s. Note: * second isomerization involves a correction (-1200 cal/mol) to account for the weaker C-H bond due to –OOH substitution.*

Addition reactions of hydroxy alkyl radicals to O_2 ($R+O_2=RO_2$) and second addition $QOOH+O_2=OOQOOH$									
	A	**n**	**Ea**	**A**	**n**	**Ea**			
	Primary radical			*Secondary radical*					
	$1.0\ 10^{12}$	0.0	0	$2.0\ 10^{12}$	0.0	0			
Recombination/disproportionation $R'+RO_2=RO+RO$ (R'=H, CH_3, alcohol radicals)									
			$3.5\ 10^{12}$	0.0	-1000				
Recombination/disproportionation $R'O_2+RO_2=RO+RO$ (R=H, CH_3, alcohol radicals)									
R=H			*R=CH 3*			*R=alcohol radicals*			
$3.0\ 10^{10}$	0.0	-1200	$2.0\ 10^{10}$	0.0	0.0	$2.0\ 10^{10}$	0.0	0.0	
RO_2 concerted eliminations to form HO_2+aldehyde/enol									
			$3.0\ 10^{37}$	0.0	39500				
RO_2 isomerizations (RO_2=QOOH)*									
1p, c5			*1p, c6*			*1s, c5*			*1s, c6*		
$1.0\ 10^{11.8}$	0.0	28500	$1.0\ 10^{11.0}$	0.0	22500	$1.0\ 10^{11.8}$	0.0	26200	$1.0\ 10^{11.0}$	0.0	22200
1s β, c5			*1s* β, c6			*1s* α, c5			*1s* α, c6		
$1.0\ 10^{11.8}$	0.0	27200	$1.0\ 10^{11.0}$	0.0	21200	$1.0\ 10^{11.8}$	0.0	24500	$1.0\ 10^{11.0}$	0.0	18500
Waddington mechanism (RO_2=OH+CH_2O+C_{n-1} aldehyde)									
			$9.0\ 10^{10.0}$	0.0	22000				
QOOH (radical in γ to OOH) decomposition to form OH+alkenes/enols+carbonyl compounds									
			$1.0\ 10^{13.2}$	0.0	22500				
QOOH (radical in β to OOH) decomposition to form HO_2+C_n Enols									
			$1.0\ 10^{14.0}$	0.0	24000				
QOOH decomposition to form OH and epoxy alcohols									
3-member cyclic structure			*4-member cyclic structure*			*5-member cyclic structure*			
$1.0\ 10^{12.0}$	0.0	18000	$1.0\ 10^{11.2}$	0.0	17000	$1.0\ 10^{10.4}$	0.0	8500	
QOOH dehydration									
			$4.0\ 10^{10.0}$	0.0	13000				
Decomposition of carbonyl hydroxyalkyl hydroperoxides (branching)									
			$1.0\ 10^{16.0}$	0.0	40000				
Decomposition of carbonyl hydroxyalkyl hydroperoxides with Korcek mechanism									
			$1.0\ 10^{2.0}$	2.13	27500				
H-abstractions on carbonyl hydroxyalkyl hydroperoxides									
	by $\dot{O}H$			*by $H\dot{O}_2$*					
	$1.0\ 10^{13.0}$	0.0	630	$5.0\ 10^{12.0}$	0.0	12460			

3. Lumping of the detailed kinetic mechanism

Simplification of detailed kinetic mechanisms through lumping techniques allows the description of complex reactive systems with a relatively limited number of species and reactions. Dente, Ranzi and co-workers [90, 91, 94] described in detail the assumptions and the algorithms underlying the application of lumping. The same techniques extensively adopted for conventional hydrocarbon fuels (e.g. *n*-alkanes, cyclo-

alkanes, *iso*-alkanes, aromatics) have been successfully applied recently also to a wide range of oxygenated fuels [20-23, 27, 51-53], including alcohols. The main issues to be tackled when applying lumping techniques are: 1) to define which species have to be lumped, 2) to determine how the species to be lumped contribute to the final lumped species and 3) to determine lumped reactions and kinetic parameters. All of the above stem from the knowledge of the detailed chemistry taking place, motivating physically meaningful choices and supporting unavoidable assumptions. Clearly, depending on the extent of the simplifications applied, some level of detail can be lost but, in the eventuality of experimental evidences shedding light on the formation of specific intermediates and products in significant quantities the reversibility of lumping can be exploited so as to increase the level of detail. However, the approach of Ranzi et al. [90] aims at reducing the number of species involved in the kinetic model while retaining very good predictive capabilities. In particular, these simplifications are of utmost convenience and importance when aiming at the development of a single kinetic model to describe the pyrolysis and oxidation of fuels from hydrogen to heavy fuel oils, including biofuels and bio-oils, as well as the formation of pollutant such as NOx and particulate matter. This is the overarching goal of the CRECK kinetic framework [62].

A detailed description of fuel radicals is retained for n-propanol (primary - γ, β, α and alkoxy radicals - RȮ) and *n*-butanol (primary - δ, secondary - γ, β, α and alkoxy - RȮ radicals), to preserve consistency with the kinetic subsets of other isomer structures developed in previous kinetic studies [51, 52]. Alkoxy radicals (RȮ) for higher molecular weight alcohols are assumed to be directly decomposed to their main β-scission products ($R_nȮ \leftrightarrow CH_2O + Ċ_{n-1}$ alkyl radical). The assumption is based on the high decomposition rate (10^8 – 10^{12} s^{-1}, T = 500 – 2000 K) of alkoxy radicals compared to β-decomposition reactions of alkyl radicals (10^2 – 10^{10} s^{-1}), on the negligibility of interactions with O_2 leading to low temperature chain branching, and on the relatively low selectivity of H-atom abstraction reactions to RȮ (< 8% for T = 500 – 2000 K) (Figure S1). Only two fuel radicals are introduced for *n*-pentanol and *n*-hexanol, one representing the alcohol specific α radical (A) and one representing the alkane moiety (B). Rate constants for H-atom abstraction reactions from the α site forming radical (A) are assigned as in Section 2.3, and its successive decomposition reactions as in Table 2.

Rate constants of H-atom abstraction reactions on the remaining sites leading to the formation of radical (B) are given by the sum $k_{abs,B} = \sum_{i=\beta}^{N} k_{abs,i}$, where N is the number of remaining carbon sites (i.e. 4 for *n*-pentanol, 5 for *n*-hexanol). Decomposition and isomerization rate constants (reaction classes 4 and 5) are obtained through the steady-state approximation at T = 1000 K as described by Ranzi et al. [90], from the reference kinetic parameters reported in Table 2. Interactions of radical (B) and (A) with O_2 forming $H\dot{O}_2$ and a C_n enol, or an aldehyde, are described as in Table 2.

Horizontal lumping is very useful to describe low temperature oxidation pathways by means of pseudo-species (lumped species) representative of the different types of intermediates: hydroxyalkyl peroxy radicals ($R\dot{O}_2$), hydroperoxyl alkyl radicals ($\dot{Q}OOH$), C_n enols, C_n epoxy alcohols, ketohydroperoxides of the parent C_n alkane, hydroxyl peroxy-hydroperoxy-alkyl radicals $\dot{O}_2QOOH$, C_n carbonyl alkyl hydroperoxides. Beside the computational advantage of this important reduction in the number of species, the introduction of one single lumped component for any intermediate radicals and compounds makes the comprehensive description of their successive reactions easier to manage and also to understand and interpret. Comprehensive kinetic mechanisms available in the literature often describe the occurring chemistry in a very detailed fashion only up until where the explosion of the number of species (e.g. in ketohydroperoxides) forces the treatment of every isomer with the same kinetic rate constant, based on analogy. This is justified by the fact that not every rate constant for every specific intermediate species has been theoretically, or experimentally determined. This coexistence of the aim for a high level of detail and difficulties in managing the complexity of combustion kinetic mechanisms, and the unavailability of specific rate constants for every isomer, further supports the suitability, efficiency, convenience and robustness of the lumped approach largely applied in previous developments of the CRECK kinetic model. The lumped kinetic parameters are then derived through an optimization process aimed at minimizing the deviation in the selectivities to final products (i.e. $\dot{Q}OOH$, $\dot{O}_2QOOH$, epoxy alcohols, enols, CHHP, etc.) between the original detailed mechanism and the lumped one, as previously described [73, 74, 81, 89-91, 94].

Decomposition reactions of CHHP via O–OH bond fission are written in a lumped way and stoichiometric coefficients are assigned to the reaction products (e.g.

$C_4CHHP \rightarrow OH+.5\dot{C}H_2CHO+.5CH_2OHCHO+.5CH_2O+.5CO+.5P\dot{C}_2H4OH$). The stoichiometric coefficients are determined at a reference intermediate temperature (T = 800 K in this case) so as to better reflect the temperature dependence of the specific channels in the low temperature branching pathways, leading to the formation of different CHHP (Figure 12) and therefore to a variable distribution of products. However, it should be noted that modifications to the relative distributions do not significantly impact the overall reactivity nor the formation of product species as the flux reaching CHHP species is typically very limited for alcohols, in particular at the conditions where experimental data are available. Figure 14 compares the distribution of products from CHHP decomposition from the reference kinetic parameters discussed in the previous section, and from the lumped model.

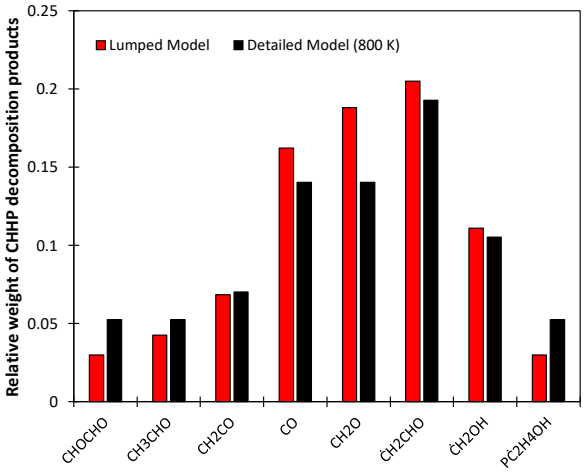

Figure 14: Relative weight of CHHP decomposition products in the lumped model and in the detailed model (T=800 K).

Table 4 shows lumped kinetic parameters for low temperature reaction pathways for *n*-propanol, *n*-butanol and *n*-pentanol. As determined by Ranzi et al. [74] for a series of *n*-alkanes it is reasonable to directly extend the kinetic parameters of *n*-pentanol to higher molecular weight alcohols (e.g. *n*-hexanol, *n*-octanol). In the case of alcohols fuel this is further justified by the decreasing importance of the alcohol specific moiety for increasing molecular weight. Concerning the first addition to O_2 ($\dot{R} + O_2 \leftrightarrow R\dot{O}_2$), for *n*-propanol and *n*-butanol the fuel radicals are described in detail in the kinetic model. Table 4 reports the sum of the individual rate constants assigned according to the reference kinetic parameters discussed in Section 2.7. For *n*-pentanol and higher molecular weight alcohols one single lumped radical (B) adds to O_2. As from the increasing carbon

chain length, one would expect that the rate constants for addition reactions rank in the order *n*-pentanol > *n*-butanol > *n*-propanol. However, according to the lumping approach adopted here [90], the rate constant for $\dot{R} + O_2$ (k_{lump}) derives from a weighted average, considering the relative branching to the different isomers (i.e. the fuel radicals) of H-abstraction reactions by $\dot{O}H$ and $H\dot{O}_2$ at the reference temperature of 700 K. Therefore, the rate constant is lower for *n*-pentanol, but the impact of the chain length is implicitly accounted for in the concentration of [$\dot{R}$], which is the sum of the concentrations of the different isomers, from which a higher addition rate is obtained as $r = k_{lump}[\dot{R}_{pentanol}][O_2]$ [mol/cm^3/s].

Table 4: Kinetic parameters of the lumped low temperature reactions of n-C_3–C_5 alcohols. Units are cm^3, mol, s, cal.

Lumped reactions	***n*-propanol**			***n*-butanol**			***n*-pentanol**		
	A	**n**	**E_a**	**A**	**n**	**E_a**	**A**	**n**	**E_a**
$R+O_2 \leftrightarrow R\dot{O}_2$*	3.0×10^{12} *3.0×10^{13}*	0.00 *0.00*	0.0 *30000.*	4.0×10^{12} *3.0×10^{13}*	0.00 *0.00*	0.0 *30000.*	1.2×10^{12} *3.0×10^{13}*	0.00 *0.00*	0.0 *30000.*
$R\dot{O}_2 \leftrightarrow \dot{Q}OOH$	1.3×10^{6} *3.4×10^{9}*	1.51 *0.29*	18449. *12513.*	4.2×10^{9} *1.8×10^{9}*	0.39 *1.60*	19621. *11124.*	2.2×10^{3} 6.0×10^{3}	2.46 2.19	17204. 10839.
$RO_2 \rightarrow \dot{O}H + CH_2O + C_{n-2}$ aldehyde (Waddington)	1.5×10^{10}	0.00	22000.	1.5×10^{10}	0.00	22000.	1.5×10^{10}	0.00	22000.
$\dot{Q}OOH$ (radical in γ to OOH) $\rightarrow$ $\dot{O}H$+alkenes/enols+carbonyl	1.0×10^{16}	−1.01	23327.	1.0×10^{16}	-1.01	23327.	$1.2\ 10^{17}$	−1.34	23538.
$\dot{Q}OOH$ (radical in β to OOH) $\rightarrow H\dot{O}_2 + C_n$ enol	5.1×10^{7}	1.82	23182.	5.1×10^{7}	1.82	23182.	5.9×10^{12}	0.48	27345.
$\dot{Q}OOH \rightarrow \dot{O}H$ + epoxy alcohols	1.7×10^{10}	0.37	17120.	2.8×10^{10}	0.37	17120.	2.8×10^{10}	0.37	17120.
$\dot{Q}OOH \rightarrow H_2O + H\dot{C}O + C_{n-1}$ aldehyde	4.0×10^{10}	0.00	13000.	4.0×10^{10}	0.00	13000.	4.0×10^{10}	0.00	13000.
α-$\dot{Q}OOH + O_2 \rightarrow H\dot{O}_2 + C_n$ alkane ketohydroperoxide	7.5×10^{10}	0.30	−1069.	7.5×10^{10}	0.30	−1069.	7.5×10^{10}	0.30	−1069.
$\dot{Q}OOH + O_2 \leftrightarrow \dot{O}_2QOOH$	2.5×10^{12} *3.0×10^{13}*	0.00 *0.00*	0.0 *30000.*	2.5×10^{12} *3.0×10^{13}*	0.00 *0.00*	0.0 *30000.*	2.5×10^{12} *3.0×10^{13}*	0.00 *0.00*	0.0 *30000.*

$\dot{O}_2$QOOH → ȮH + carbonyl hydroxyalkyl hydroperoxides	1.3×10^{6}	1.51	17249.	4.2×10^{9}	0.4	18421.	2.2×10^{3}	2.5	16004.
carbonyl hydroxyalkyl hydroperoxides → ȮH + radicals	$1. \times 10^{16}$	0.0	40000.	$1. \times 10^{16}$	0.0	40000.	1.0×10^{16}	0.0	40000.

*Notes: 1) * detailed fuel radicals (R) description for n-propanol and n-butanol, rate parameters reported in Table are the sum of the individual rate constants. 2) Reverse lumped rate constants in italics.*

Figure 15 demonstrates the validity of the lumping approach described above by comparing the profiles of relevant species in the low temperature oxidation pathways of *n*-pentanol obtained with the detailed kinetic model of Sarathy et al. [5] and with the lumped kinetic model presented in this work. Results are obtained from a simulation in an adiabatic constant volume batch reactor. The two models predict very similar values of the IDT (≈ 9.4 ms) at $T = 900$ K, $p = 10$ bar and $\varphi = 1.0$. The minor difference in the fuel conversion profiles, justified by slightly different rate constants for the H-atom abstraction reactions, is responsible for the differences in the mole fraction profiles of intermediate species at early times preceding the ignition event.

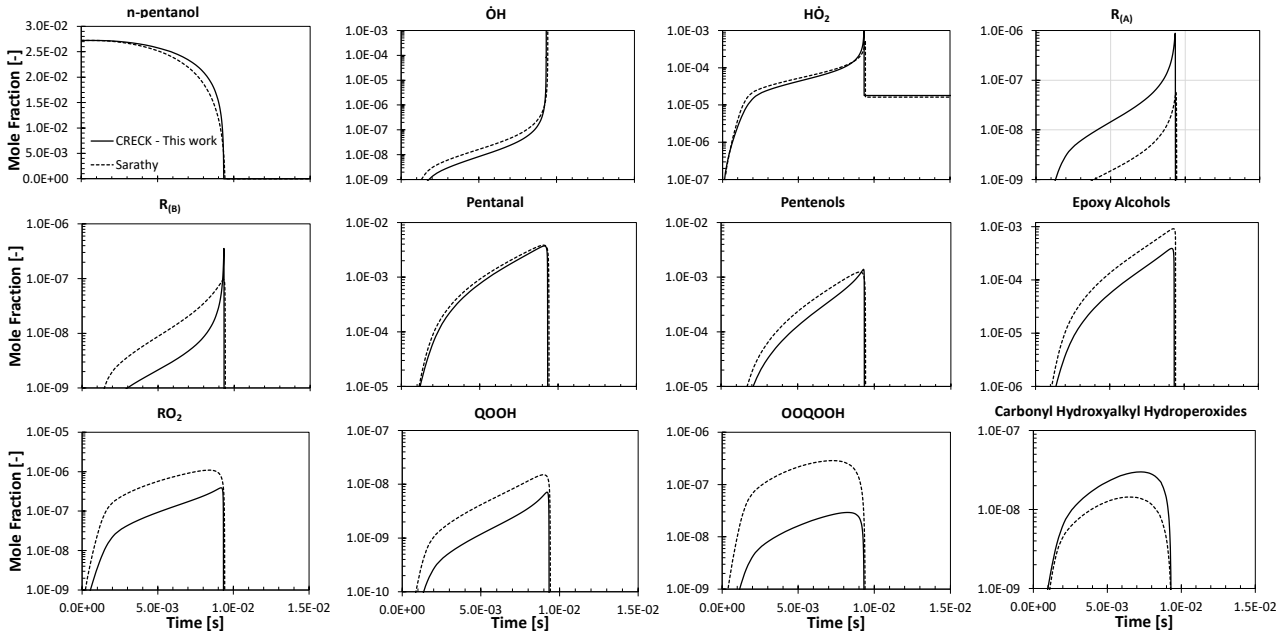

Figure 15: Simulated mole fraction profiles of relevant species in the oxidation of an n-pentanol/air mixture in an adiabatic constant volume batch reactor (T = 900 K, p = 10 bar, φ = 1.0). Solid lines: lumped model from this work, dashed lines: detailed model from Sarathy et al. [5].

$H\dot{O}_2$ radicals are produced by the interaction of O_2 with α radicals, forming *n*-pentanal, and is consumed by H-atom abstraction from the fuel molecule, and by the termination reaction $H\dot{O}_2 + H\dot{O}_2 = H_2O_2 + O_2$, further decomposition of H_2O_2 producing two ȮH radicals drives the onset of ignition. Despite similar shapes, our lumped model predicts higher yields of α radicals (≈ 1 order of magnitude) and lower yields of the remaining alkyl radicals. This difference propagates throughout the low temperature branching pathways that mostly derives from the oxidation of the remaining alkyl radicals. Indeed, the model of Sarathy predicts higher yields of $R\dot{O}_2$, ȮOOH, epoxy alcohols and $\dot{O}_2$QOOH. Figure 16 shows a rate of production analysis at 20% fuel conversion for the same conditions of Figure 15.

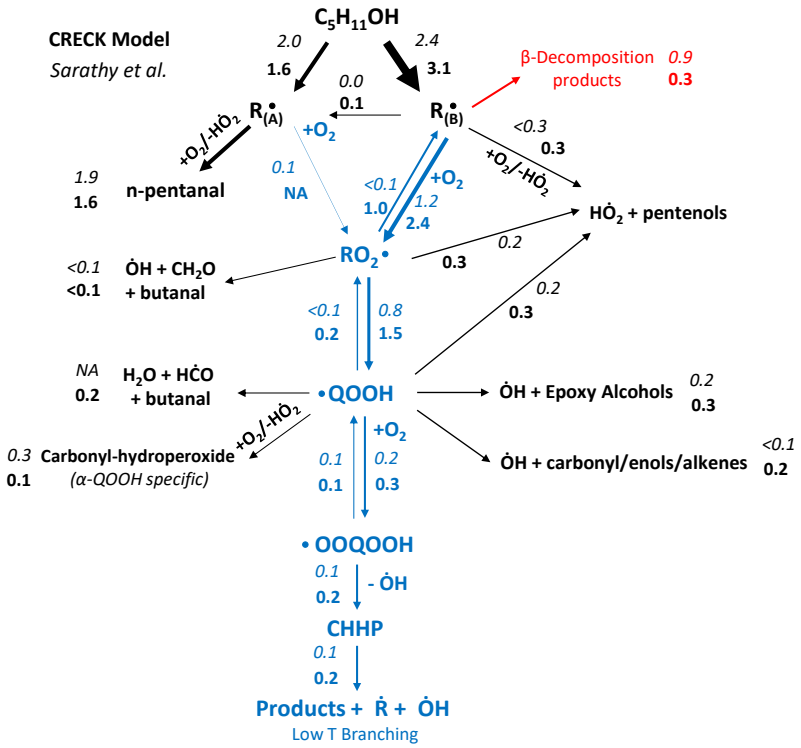

Figure 16: flux analysis of n-pentanol oxidation in an adiabatic constant volume batch reactor at T = 900 K, p = 10 bar and φ = 1.0 (fuel conversion ~20%). Numbers are rates of production/consumption in 10^{-4} mol cm^{-3} s^{-1}. Bold: CRECK model, italics: Sarathy et al. [5]. *NA = pathway not available in the model.*

The different isomers of the low temperature branching pathways described in detail by Sarathy et al. [5] (77 species) have been grouped so as to resemble the lumped species (9 species). The main differences between the two kinetic models arise from the selectivity of H-atom abstraction reactions. The selectivity to α-radical $R_{(A)}$ is 35% for our model and 45% in the model of Sarathy et al. Nearly all the formed $R_{(A)}$ is converted to *n*-pentanal in the CRECK model, while about 5% adds to O_2 producing $R\dot{O}_2$ according to Sarathy. Different rate parameters justify the higher importance of β-scission reactions in Sarathy et al. (Figure S1), while our kinetic model proposes a preferential addition to O_2 towards the low temperature chain branching pathways. This effect is counterbalanced by higher backward rates for $R\dot{O}_2 = \dot{R} + O_2$ and by a higher formation of pentenol isomers and $H\dot{O}_2$ radicals. A minor difference is also observed for the isomerization reactions leading to $\dot{R}_{(A)}$. $R\dot{O}_2$ radicals mostly isomerize to $\dot{Q}OOH$ in both models with the CRECK model predicting a higher flux of the backward reaction. Similar fluxes are observed for the decomposition of $R\dot{O}_2$ to $H\dot{O}_2$ and the pentenol isomers. The low importance of the Waddington mechanism producing ȮH, formaldehyde and *n*-butanal is consistent between the two models. Due to the relatively high temperature conditions the second addition

to O_2 ($\dot{Q}OOH + O_2 = \dot{O}_2QOOH$) is of minor importance compared to $\dot{Q}OOH$ decomposition pathways (20% vs 80%). The same flux is then conserved until the branching decomposition reactions of CHHP.

From this graphical representation it is possible to conclude that: 1) the CRECK model proposes a higher influence of the chemical equilibrium in the low temperature branching pathways, thus justifying the differences in the yields of $R\dot{O}_2$, $\dot{Q}OOH$ and $\dot{O}_2QOOH$ highlighted in Figure 15; 2) the higher flux undergoing the low temperature branching pathway in the CRECK model is counter balanced by a higher importance of backwards reactions and propagation pathways such as the decompositions of $\dot{Q}OOH$ and $R\dot{O}_2$ radicals. Globally, the similar balance between branching and propagation pathways justifies the similar reactivity. A similar analysis, for lower temperature conditions (T = 748 K) is reported in the Supplementary material (Figure S2), further supporting the governing role of relative contributions in terms of global reactive fluxes between competing pathways (e.g. low temperature branching vs propagation/termination reactions) rather than the absolute values of rate constants when the goal is to reproduce macroscopic targets such as IDTs. The satisfactory agreement of the lumped model here proposed with detailed speciation data over a wide range of conditions for the different fuels further supports the selected parameters and the reliability of the simplifications here proposed.

4. Preliminary model validation

Due to space limitation, in this Section, we only present a synopsis of the overall performances of the model (Table 5). A detailed description of the experimental set-ups of the jet-stirred reactor and of the rapid compression machine used in this study are presented in Part II [56] together with a more detailed discussion on model validation and performances. Model simulations have been performed using the OpenSMOKE++ solvers by Cuoci et al. [95].

Table 5: Synopsis of validation targets and model performances. For a deeper discussion the reader is referred to Part II of this study [56].

Reference	Exp. Device	Example of results
Pyrolysis Speciation, Hefei [54, 55, 83]	Flow reactor, Molecular beam mass spectrometry	*T = 900 – 1400 K, p = 150 – 200 Torr, φ = ∞, 3% mol fuel/Ar.* 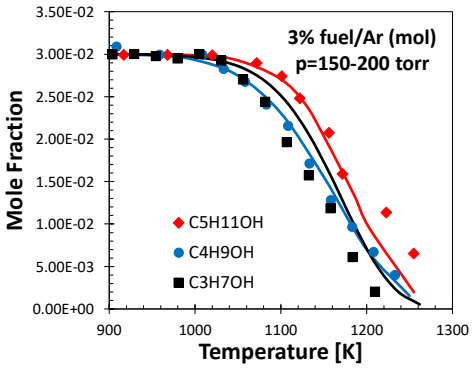
Pyrolysis Speciation, Ghent [37, 59]	Flow Reactor, gas chromatography	*T = 640 – 810 °C, p = 1.7 bar, φ = ∞, 50% mol fuel/N_2.* 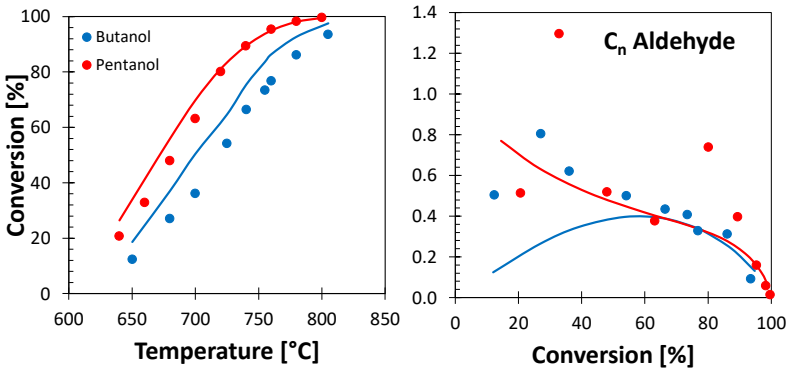
Laminar Flame Speed [54, 60, 61, 96-98]	Constant volume combustion vessel, Heat Flux Burner	*T = 423 K, p = 1 atm, φ = 0.7 – 1.7.* 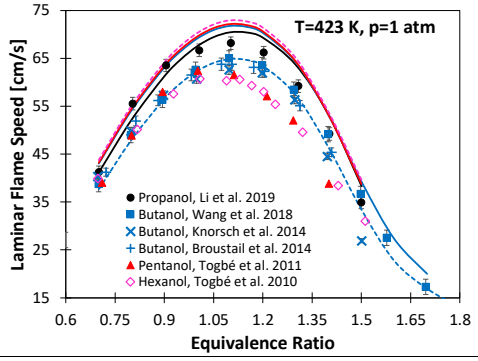
Ignition Delay Time [50, 99-103]	Shock tube	*T = 700 – 1700 K, p = 1 – 30 bar, φ = 0.25 – 2.00.* 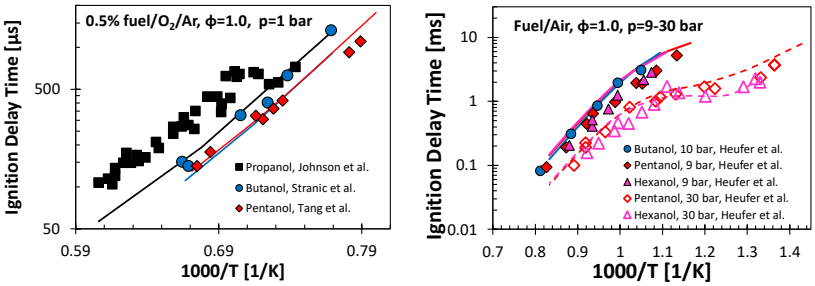
Ignition Delay Time [56, 104]	Rapid Compression Machine	*T = 650 – 950 K, p = 10 bar, φ = 1.0.*

		Fuel in "Air", ϕ=1.0, p=10 bar 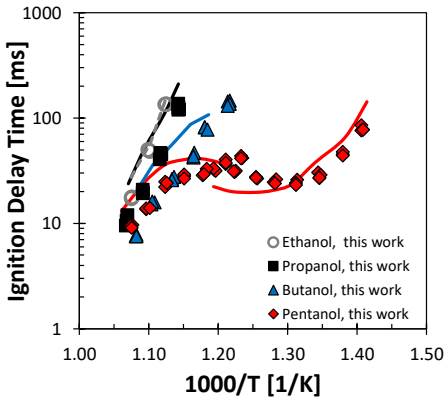
Oxidation speciation, JSR Nancy [56]	Jet Stirred Reactor, gas chromatography mass spectrometry (GC-MS)	*T = 500 – 1100 K, p = 1.07 bar, φ = 1.0 (0.5% mol fuel/O_2/He), τ = 2.0 s.* 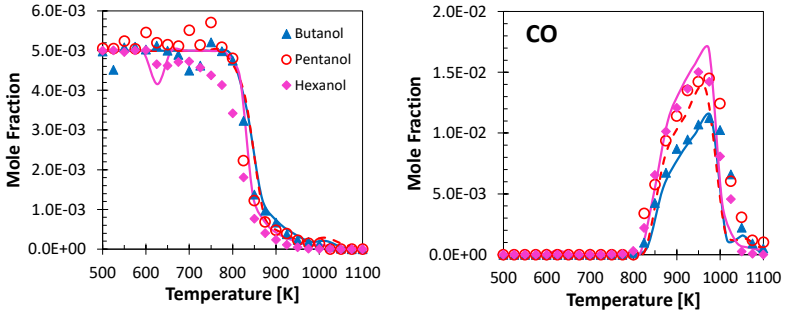
Oxidation speciation, JSR Orleans [58, 60, 61, 72]	Jet Stirred Reactor, gas chromatography mass spectrometry (GC-MS)	*T = 550 – 1150 K, p = 10 bar, φ = 0.5 (0.1% mol fuel/O_2/N_2), τ = 0.7 s.* 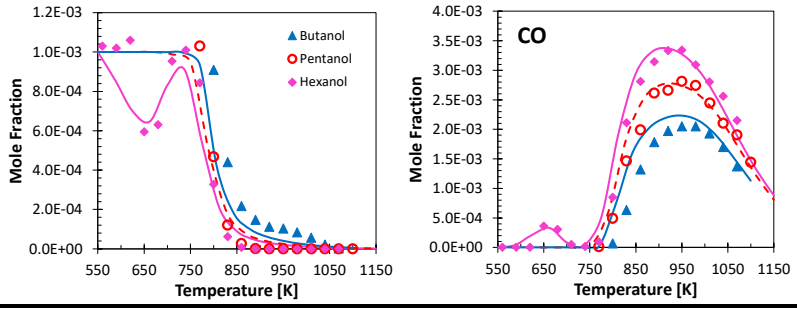

5. Conclusions

Considering new experimental measurements carried out in this work (see Part II [56]), as well as the large amount of experimental data on alcohols pyrolysis and combustion available in the literature, the alcohol subset of the CRECK kinetic model developed in previous kinetics studies [51-53] has been updated and systematically extended to describe the low temperature oxidation of *n*-butanol, *n*-pentanol and *n*-hexanol at low temperatures. The kinetic model is developed based on the reaction class and rate rules approach, and a thorough discussion of the different classes and of the reference kinetic parameters is provided. The underlying assumption upon which the model has been developed is that it is possible to simplify the description of alcohol fuels from *n*-propanol assuming an alkane-like moiety and an alcohol-

specific moiety. Based on a recent review [5] and on previous theoretical and kinetic modeling studies, reference kinetic parameters for alcohols specific reaction pathways have been defined also correcting rate rules for alkane fuels by taking into account the peculiar features (e.g. BDE) induced by the presence of the hydroxyl function. The reference kinetic parameters thus defined have been systematically applied to the entire *n*-$C_3 - C_6$ alcohol series, and the application of lumping techniques allowed us to obtain an effective and compact description. As a further proof of concept the same approach has been further extended to *n*-octanol (see Part II [56]). The model obtained generally shows good agreement over the wide range of conditions considered for the validation. The CRECK model attached to this study also describes the oxidation of other real fuel components (*n*-alkanes, *iso*-alkanes, aromatics, cyclo-alkanes, etc.) and the formation of pollutants (NOx, PAHs, soot) thus constituting a useful tool for fuel design.

Acknowledgements

The authors at Politecnico di Milano and CNRS-Nancy acknowledge the financial support of IMPROOF project (H2020-IND-CE-2016-17/H2020-SPIRE-S016) European Union's Horizon 2020 research and innovation program (grant agreement no. 723706). The authors from NUI Galway acknowledge funding from Science Foundation Ireland (SFI) via project numbers 15/IA/3177 and 16/SP/3829.

References

[1] O.I. Awad, R. Mamat, O.M. Ali, N. Sidik, T. Yusaf, K. Kadirgama, M. Kettner, Alcohol and ether as alternative fuels in spark ignition engine: A review, Renewable and Sustainable Energy Reviews 82 (2018) 2586-2605.
[2] K. Kohse-Höinghaus, P. Oßwald, T.A. Cool, T. Kasper, N. Hansen, F. Qi, C.K. Westbrook, P.R. Westmoreland, Biofuel combustion chemistry: from ethanol to biodiesel, Angewandte Chemie International Edition 49 (2010) 3572-3597.
[3] G.T. Kalghatgi, The outlook for fuels for internal combustion engines, International Journal of Engine Research 15 (2014) 383-398.
[4] N. Morgan, A. Smallbone, A. Bhave, M. Kraft, R. Cracknell, G. Kalghatgi, Mapping surrogate gasoline compositions into RON/MON space, Combustion and Flame 157 (2010) 1122-1131.
[5] S.M. Sarathy, P. Oßwald, N. Hansen, K. Kohse-Höinghaus, Alcohol combustion chemistry, Progress in energy and Combustion Science 44 (2014) 40-102.
[6] M.J. Murphy, J.D. Taylor, R.L. McCormick, Compendium of experimental cetane number data, National Renewable Energy Laboratory Golden, CO2004.
[7] S. Saravanan, Effect of exhaust gas recirculation (EGR) on performance and emissions of a constant speed DI diesel engine fueled with pentanol/diesel blends, Fuel 160 (2015) 217-226.
[8] L. Cai, Y. Uygun, C. Togbé, H. Pitsch, H. Olivier, P. Dagaut, S.M. Sarathy, An experimental and modeling study of n-octanol combustion, Proceedings of the Combustion Institute 35 (2015) 419-427.

[9] B.R. Kumar, S. Saravanan, Effects of iso-butanol/diesel and n-pentanol/diesel blends on performance and emissions of a DI diesel engine under premixed LTC (low temperature combustion) mode, Fuel 170 (2016) 49-59.
[10] L. Wei, C. Cheung, Z. Huang, Effect of n-pentanol addition on the combustion, performance and emission characteristics of a direct-injection diesel engine, Energy 70 (2014) 172-180.
[11] D. Babu, R. Anand, Effect of biodiesel-diesel-n-pentanol and biodiesel-diesel-n-hexanol blends on diesel engine emission and combustion characteristics, Energy 133 (2017) 761-776.
[12] L. Zhu, Y. Xiao, C. Cheung, C. Guan, Z. Huang, Combustion, gaseous and particulate emission of a diesel engine fueled with n-pentanol (C5 alcohol) blended with waste cooking oil biodiesel, Applied Thermal Engineering 102 (2016) 73-79.
[13] H. Chen, X. Su, J. He, B. Xie, Investigation on combustion and emission characteristics of a common rail diesel engine fueled with diesel/n-pentanol/methanol blends, Energy 167 (2019) 297-311.
[14] L. Li, J. Wang, Z. Wang, J. Xiao, Combustion and emission characteristics of diesel engine fueled with diesel/biodiesel/pentanol fuel blends, Fuel 156 (2015) 211-218.
[15] M.V. De Poures, A. Sathiyagnanam, D. Rana, B.R. Kumar, S. Saravanan, 1-Hexanol as a sustainable biofuel in DI diesel engines and its effect on combustion and emissions under the influence of injection timing and exhaust gas recirculation (EGR), Applied Thermal Engineering 113 (2017) 1505-1513.
[16] B.R. Kumar, S. Saravanan, D. Rana, A. Nagendran, A comparative analysis on combustion and emissions of some next generation higher-alcohol/diesel blends in a direct-injection diesel engine, Energy conversion and management 119 (2016) 246-256.
[17] M. Pelucchi, M. Bissoli, C. Rizzo, Y. Zhang, K. Somers, A. Frassoldati, H. Curran, T. Faravelli, A kinetic modelling study of alcohols operating regimes in a HCCI engine, SAE International Journal of Engines 10 (2017) 2354-2370.
[18] H.J. Curran, Developing detailed chemical kinetic mechanisms for fuel combustion, Proceedings of the Combustion Institute 37 (2019) 57-81.
[19] K.P. Somers, R.F. Cracknell, H.J. Curran, A chemical kinetic interpretation of the octane appetite of modern gasoline engines, Proceedings of the Combustion Institute 37 (2019) 4857-4864.
[20] M. Pelucchi, C. Cavallotti, E. Ranzi, A. Frassoldati, T. Faravelli, Relative reactivity of oxygenated fuels: alcohols, aldehydes, ketones, and methyl esters, Energy & Fuels 30 (2016) 8665-8679.
[21] M. Pelucchi, S. Namysl, E. Ranzi, A. Frassoldati, O. Herbinet, F. Battin-Leclerc, T. Faravelli, An experimental and kinetic modelling study of n-C4C6 aldehydes oxidation in a jet-stirred reactor, Proceedings of the Combustion Institute 37 (2019) 389-397.
[22] M. Pelucchi, E. Ranzi, A. Frassoldati, T. Faravelli, Alkyl radicals rule the low temperature oxidation of long chain aldehydes, Proceedings of the Combustion Institute 36 (2017) 393-401.
[23] M. Pelucchi, K.P. Somers, K. Yasunaga, U. Burke, A. Frassoldati, E. Ranzi, H.J. Curran, T. Faravelli, An experimental and kinetic modeling study of the pyrolysis and oxidation of n-C3C5 aldehydes in shock tubes, Combustion and Flame 162 (2015) 265-286.
[24] P.S. Veloo, P. Dagaut, C. Togbe, G. Dayma, S. Sarathy, C.K. Westbrook, F.N. Egolfopoulos, Jet-stirred reactor and flame studies of propanal oxidation, Proceedings of the Combustion Institute 34 (2013) 599-606.
[25] P.S. Veloo, P. Dagaut, C. Togbé, G. Dayma, S.M. Sarathy, C.K. Westbrook, F.N. Egolfopoulos, Experimental and modeling study of the oxidation of n-and iso-butanal, Combustion and flame 160 (2013) 1609-1626.
[26] S. Namysl, M. Pelucchi, O. Herbinet, A. Frassoldati, T. Faravelli, F. Battin-Leclerc, A first evaluation of butanoic and pentanoic acid oxidation kinetics, Chemical Engineering Journal 373 (2019) 973-984.
[27] M. Pelucchi, C. Cavallotti, A. Cuoci, T. Faravelli, A. Frassoldati, E. Ranzi, Detailed kinetics of substituted phenolic species in pyrolysis bio-oils, Reaction Chemistry & Engineering 4 (2019) 490-506.
[28] S. Namysl, M. Pelucchi, L.P. Maffei, O. Herbinet, A. Stagni, T. Faravelli, F. Battin-Leclerc, Experimental and modeling study of benzaldehyde oxidation, Combustion and Flame 211 (2020) 124-132.
[29] L.P. Maffei, M. Pelucchi, T. Faravelli, C. Cavallotti, Theoretical study of sensitive reactions in phenol decomposition, Reaction Chemistry & Engineering, (2020).

[30] M. Bertero, G. de la Puente, U. Sedran, Fuels from bio-oils: Bio-oil production from different residual sources, characterization and thermal conditioning, Fuel 95 (2012) 263-271.
[31] G. da Silva, J.W. Bozzelli, Role of the α-hydroxyethylperoxy radical in the reactions of acetaldehyde and vinyl alcohol with HO2, Chemical Physics Letters 483 (2009) 25-29.
[32] G. da Silva, J.W. Bozzelli, L. Liang, J.T. Farrell, Ethanol oxidation: Kinetics of the α-hydroxyethyl radical+ O2 reaction, The Journal of Physical Chemistry A 113 (2009) 8923-8933.
[33] B. Aazaad, S. Lakshmipathi, Reaction of Pentanol isomers with OH radical–A theoretical perspective, Molecular Physics 116 (2018) 1153-1165.
[34] J. Daranlot, A. Bergeat, F. Caralp, P. Caubet, M. Costes, W. Forst, J.C. Loison, K.M. Hickson, Gas-Phase Kinetics of Hydroxyl Radical Reactions with Alkenes: Experiment and Theory, ChemPhysChem 11 (2010) 4002-4010.
[35] D. Ferro-Costas, E. Martínez-Núñez, J. Rodríguez-Otero, E. Cabaleiro-Lago, C.M. Estévez, B. Fernández, A. Fernández-Ramos, S.A. Vázquez, Influence of multiple conformations and paths on rate constants and product branching ratios. thermal decomposition of 1-propanol radicals, The Journal of Physical Chemistry A 122 (2018) 4790-4800.
[36] X. Guo, R.M. Zhang, L.G. Gao, X. Zhang, X. Xu, Computational kinetics of the hydrogen abstraction reactions of n-propanol and iso-propanol by OH radical, Physical Chemistry Chemical Physics 21 (2019) 24458-24468.
[37] R. Van de Vijver, K.M. Van Geem, G.B. Marin, J. Zádor, Decomposition and isomerization of 1-pentanol radicals and the pyrolysis of 1-pentanol, Combustion and Flame 196 (2018) 500-514.
[38] J. Zádor, R.X. Fernandes, Y. Georgievskii, G. Meloni, C.A. Taatjes, J.A. Miller, The reaction of hydroxyethyl radicals with O2: A theoretical analysis and experimental product study, Proceedings of the Combustion Institute 32 (2009) 271-277.
[39] J. Mendes, C.-W. Zhou, H.J. Curran, Theoretical study of the rate constants for the hydrogen atom abstraction reactions of esters with• OH radicals, The Journal of Physical Chemistry A 118 (2014) 4889-4899.
[40] O. Welz, S.J. Klippenstein, L.B. Harding, C.A. Taatjes, J. Zádor, Unconventional peroxy chemistry in alcohol oxidation: the water elimination pathway, The journal of physical chemistry letters 4 (2013) 350-354.
[41] C.W. Zhou, J.M. Simmie, H.J. Curran, Rate constants for hydrogen abstraction by HȮ2 from n-butanol, International Journal of Chemical Kinetics 44 (2012) 155-164.
[42] D. Katsikadakos, C.-W. Zhou, J. Simmie, H. Curran, P. Hunt, Y. Hardalupas, A. Taylor, Rate constants of hydrogen abstraction by methyl radical from n-butanol and a comparison of CanTherm, MultiWell and Variflex, Proceedings of the Combustion Institute 34 (2013) 483-491.
[43] C.-W. Zhou, J.M. Simmie, H.J. Curran, Rate constants for hydrogen-abstraction by O˙ H from n-butanol, Combustion and Flame 158 (2011) 726-731.
[44] M.R. McGillen, M. Baasandorj, J.B. Burkholder, Gas-phase rate coefficients for the OH+ n-, i-, s-, and t-butanol reactions measured between 220 and 380 K: Non-arrhenius behavior and site-specific reactivity, The Journal of Physical Chemistry A 117 (2013) 4636-4656.
[45] G.A. Pang, R.K. Hanson, D.M. Golden, C.T. Bowman, Rate constant measurements for the overall reaction of OH+ 1-butanol→ products from 900 to 1200 K, The Journal of Physical Chemistry A 116 (2012) 2475-2483.
[46] B. Rajakumar, D.C. McCabe, R.K. Talukdar, A. Ravishankara, Rate coefficients for the reactions of OH with n-propanol and iso-propanol between 237 and 376 K, International Journal of Chemical Kinetics 42 (2010) 10-24.
[47] R. Sivaramakrishnan, M.-C. Su, J. Michael, S. Klippenstein, L. Harding, B. Ruscic, Rate constants for the thermal decomposition of ethanol and its bimolecular reactions with OH and D: reflected shock tube and theoretical studies, The Journal of Physical Chemistry A 114 (2010) 9425-9439.
[48] M. Yujing, A. Mellouki, Temperature dependence for the rate constants of the reaction of OH radicals with selected alcohols, Chemical Physics Letters 333 (2001) 63-68.
[49] S.S. Vasu, D.F. Davidson, R.K. Hanson, D.M. Golden, Measurements of the reaction of OH with n-butanol at high-temperatures, Chemical Physics Letters 497 (2010) 26-29.

[50] K.A. Heufer, S.M. Sarathy, H.J. Curran, A.C. Davis, C.K. Westbrook, W.J. Pitz, Detailed kinetic modeling study of n-pentanol oxidation, Energy & Fuels 26 (2012) 6678-6685.
[51] A. Frassoldati, A. Cuoci, T. Faravelli, U. Niemann, E. Ranzi, R. Seiser, K. Seshadri, An experimental and kinetic modeling study of n-propanol and iso-propanol combustion, Combustion and Flame 157 (2010) 2-16.
[52] R. Grana, A. Frassoldati, T. Faravelli, U. Niemann, E. Ranzi, R. Seiser, R. Cattolica, K. Seshadri, An experimental and kinetic modeling study of combustion of isomers of butanol, Combustion and Flame 157 (2010) 2137-2154.
[53] D. Nativel, M. Pelucchi, A. Frassoldati, A. Comandini, A. Cuoci, E. Ranzi, N. Chaumeix, T. Faravelli, Laminar flame speeds of pentanol isomers: An experimental and modeling study, Combustion and Flame 166 (2016) 1-18.
[54] W. Li, Y. Zhang, B. Mei, Y. Li, C. Cao, J. Zou, J. Yang, Z. Cheng, Experimental and kinetic modeling study of n-propanol and i-propanol combustion: Flow reactor pyrolysis and laminar flame propagation, Combustion and Flame 207 (2019) 171-185.
[55] G. Wang, W. Yuan, Y. Li, L. Zhao, F. Qi, Experimental and kinetic modeling study of n-pentanol pyrolysis and combustion, Combustion and Flame 162 (2015) 3277-3287.
[56] M. Pelucchi, S. Namysl, E. Ranzi, A. Rodriguez, C. Rizzo, K. Somers, Y. Zhang, O. Herbinet, H. Curran, F. Battin-Leclerc, T. Faravelli, Combustion of n-C3–C6 linear alcohols: an experimental and kinetic modeling study. Part II: speciation measurement in a jet stirred reactor, ignition delay time measurement in a rapid compression machine, model validation and kinetic analysis. , Submitted to Energy and Fuels, (2020).
[57] G. Black, H. Curran, S. Pichon, J. Simmie, V. Zhukov, Bio-butanol: Combustion properties and detailed chemical kinetic model, Combustion and Flame 157 (2010) 363-373.
[58] P. Dagaut, S. Sarathy, M. Thomson, A chemical kinetic study of n-butanol oxidation at elevated pressure in a jet stirred reactor, Proceedings of the combustion Institute 32 (2009) 229-237.
[59] M.R. Harper, K.M. Van Geem, S.P. Pyl, G.B. Marin, W.H. Green, Comprehensive reaction mechanism for n-butanol pyrolysis and combustion, Combustion and Flame 158 (2011) 16-41.
[60] C. Togbé, F. Halter, F. Foucher, C. Mounaïm-Rousselle, P. Dagaut, Experimental and detailed kinetic modeling study of 1-pentanol oxidation in a JSR and combustion in a bomb, Proceedings of the Combustion Institute 33 (2011) 367-374.
[61] C. Togbe, P. Dagaut, A. Mzé-Ahmed, P. Diévart, F. Halter, F. Foucher, Experimental and detailed kinetic modeling study of 1-hexanol oxidation in a pressurized jet-stirred reactor and a combustion bomb, Energy & fuels 24 (2010) 5859-5875.
[62] T. Faravelli, A. Frassoldati, A. Cuoci, M. Mehl, M. Pelucchi, A. Stagni, E. Ranzi, CRECK Modeling Lab. http://creckmodeling.chem.polimi.it/menu-kinetics/ 2020).
[63] W. Pejpichestakul, E. Ranzi, M. Pelucchi, A. Frassoldati, A. Cuoci, A. Parente, T. Faravelli, Examination of a soot model in premixed laminar flames at fuel-rich conditions, Proceedings of the Combustion Institute 37 (2019) 1013-1021.
[64] Y. Song, L. Marrodán, N. Vin, O. Herbinet, E. Assaf, C. Fittschen, A. Stagni, T. Faravelli, M. Alzueta, F. Battin-Leclerc, The sensitizing effects of NO2 and NO on methane low temperature oxidation in a jet stirred reactor, Proceedings of the Combustion Institute 37 (2019) 667-675.
[65] W.K. Metcalfe, S.M. Burke, S.S. Ahmed, H.J. Curran, A hierarchical and comparative kinetic modeling study of C1− C2 hydrocarbon and oxygenated fuels, International Journal of Chemical Kinetics 45 (2013) 638-675.
[66] A. Kéromnès, W.K. Metcalfe, K.A. Heufer, N. Donohoe, A.K. Das, C.-J. Sung, J. Herzler, C. Naumann, P. Griebel, O. Mathieu, An experimental and detailed chemical kinetic modeling study of hydrogen and syngas mixture oxidation at elevated pressures, Combustion and Flame 160 (2013) 995-1011.
[67] S.M. Burke, W. Metcalfe, O. Herbinet, F. Battin-Leclerc, F.M. Haas, J. Santner, F.L. Dryer, H.J. Curran, An experimental and modeling study of propene oxidation. Part 1: Speciation measurements in jet-stirred and flow reactors, Combustion and Flame 161 (2014) 2765-2784.
[68] G. Bagheri, E. Ranzi, M. Pelucchi, A. Parente, A. Frassoldati, T. Faravelli, Comprehensive kinetic study of combustion technologies for low environmental impact: MILD and OXY-fuel combustion of methane, Combustion and flame 212 (2020) 142-155.

[69] B. Ruscic, Uncertainty quantification in thermochemistry, benchmarking electronic structure computations, and Active Thermochemical Tables, International Journal of Quantum Chemistry 114 (2014) 1097-1101.
[70]
B. Ruscic, R.E. Pinzon, G. Von Laszewski, D. Kodeboyina, A. Burcat, D. Leahy, D. Montoy, A.F. Wagner. Active Thermochemical Tables: thermochemistry for the 21st century. In: editor^editors. Journal of Physics: Conference Series; 2005: IOP Publishing. p. 561.
[71] S.W. Benson, J.H. Buss, Additivity rules for the estimation of molecular properties. Thermodynamic properties, The Journal of Chemical Physics 29 (1958) 546-572.
[72] S.M. Sarathy, M.J. Thomson, C. Togbé, P. Dagaut, F. Halter, C. Mounaim-Rousselle, An experimental and kinetic modeling study of n-butanol combustion, Combustion and Flame 156 (2009) 852-864.
[73] E. Ranzi, C. Cavallotti, A. Cuoci, A. Frassoldati, M. Pelucchi, T. Faravelli, New reaction classes in the kinetic modeling of low temperature oxidation of n-alkanes, Combustion and flame 162 (2015) 1679-1691.
[74] E. Ranzi, A. Frassoldati, S. Granata, T. Faravelli, Wide-range kinetic modeling study of the pyrolysis, partial oxidation, and combustion of heavy n-alkanes, Industrial & engineering chemistry research 44 (2005) 5170-5183.
[75] X. Man, C. Tang, J. Zhang, Y. Zhang, L. Pan, Z. Huang, C.K. Law, An experimental and kinetic modeling study of n-propanol and i-propanol ignition at high temperatures, Combustion and flame 161 (2014) 644-656.
[76] V.B. Oyeyemi, J.A. Keith, E.A. Carter, Trends in bond dissociation energies of alcohols and aldehydes computed with multireference averaged coupled-pair functional theory, The Journal of Physical Chemistry A 118 (2014) 3039-3050.
[77] V.B. Oyeyemi, D.B. Krisiloff, J.A. Keith, F. Libisch, M. Pavone, E.A. Carter, Size-extensivity-corrected multireference configuration interaction schemes to accurately predict bond dissociation energies of oxygenated hydrocarbons, The Journal of chemical physics 140 (2014) 044317.
[78] L. Zhao, L. Ye, F. Zhang, L. Zhang, Thermal decomposition of 1-pentanol and its isomers: A theoretical study, The Journal of Physical Chemistry A 116 (2012) 9238-9244.
[79] E. Ranzi, P. Gaffuri, T. Faravelli, P. Dagaut, A wide-range modeling study of n-heptane oxidation, Combustion and Flame 103 (1995) 91-106.
[80] H.J. Curran, P. Gaffuri, W.J. Pitz, C.K. Westbrook, A comprehensive modeling study of n-heptane oxidation, Combustion and flame 114 (1998) 149-177.
[81] E. Ranzi, M. Dente, S. Pierucci, G. Biardi, Initial product distributions from pyrolysis of normal and branched paraffins, Industrial & Engineering Chemistry Fundamentals 22 (1983) 132-139.
[82] C.M. Rosado-Reyes, W. Tsang, Shock tube study on the thermal decomposition of n-butanol, The Journal of Physical Chemistry A 116 (2012) 9825-9831.
[83] J. Cai, L. Zhang, F. Zhang, Z. Wang, Z. Cheng, W. Yuan, F. Qi, Experimental and kinetic modeling study of n-butanol pyrolysis and combustion, Energy & fuels 26 (2012) 5550-5568.
[84] J. Cai, W. Yuan, L. Ye, Z. Cheng, Y. Wang, L. Zhang, F. Zhang, Y. Li, F. Qi, Experimental and kinetic modeling study of 2-butanol pyrolysis and combustion, Combustion and flame 160 (2013) 1939-1957.
[85] E. Ranzi, A. Sogaro, P. Gaffuri, G. Pennati, T. Faravelli, A wide range modeling study of methane oxidation, Combustion science and technology 96 (1994) 279-325.
[86] E. Ranzi, M. Dente, T. Faravelli, G. Pennati, Prediction of kinetic parameters for hydrogen abstraction reactions, Combustion science and technology 95 (1993) 1-50.
[87] K. Oganesyan, A. Nalbandyan, Determination fo the rate constant for the reaction of atomic hydrogen with propyl and butyl alcohols, Izv Akad Nauk Arm SSR Khim Nauki, (1965).
[88] P. Zhang, S.J. Klippenstein, C.K. Law, Ab initio kinetics for the decomposition of hydroxybutyl and butoxy radicals of n-butanol, The Journal of Physical Chemistry A 117 (2013) 1890-1906.
[89] M. Dente, G. Bozzano, T. Faravelli, A. Marongiu, S. Pierucci, E. Ranzi, Kinetic modelling of pyrolysis processes in gas and condensed phase, Advances in chemical engineering 32 (2007) 51-166.
[90] E. Ranzi, M. Dente, A. Goldaniga, G. Bozzano, T. Faravelli, Lumping procedures in detailed kinetic modeling of gasification, pyrolysis, partial oxidation and combustion of hydrocarbon mixtures, Progress in Energy and Combustion Science 27 (2001) 99-139.

[91] E. Ranzi, A. Frassoldati, A. Stagni, M. Pelucchi, A. Cuoci, T. Faravelli, Reduced kinetic schemes of complex reaction systems: fossil and biomass-derived transportation fuels, International Journal of Chemical Kinetics 46 (2014) 512-542.
[92] D. Ray, D. Waddington, Gas phase oxidation of alkenes—Part II. The oxidation of 2-methylbutene-2 and 2, 3-dimethylbutene-2, Combustion and Flame 20 (1973) 327-334.
[93] Y. Li, Q. Zhao, Y. Zhang, Z. Huang, S.M. Sarathy, A Systematic Theoretical Kinetics Analysis for the Waddington Mechanism in the Low-Temperature Oxidation of Butene and Butanol Isomers, The Journal of Physical Chemistry A 124 (2020) 5646-5656.
[94] E. Ranzi, T. Faravelli, P. Gaffuri, A. Sogaro, Low-temperature combustion: automatic generation of primary oxidation reactions and lumping procedures, Combustion and flame 102 (1995) 179-192.
[95] A. Cuoci, A. Frassoldati, T. Faravelli, E. Ranzi, OpenSMOKE++: An object-oriented framework for the numerical modeling of reactive systems with detailed kinetic mechanisms, Computer Physics Communications 192 (2015) 237-264.
[96] G. Wang, Y. Li, W. Yuan, Y. Wang, Z. Zhou, Y. Liu, J. Cai, Investigation on laminar flame propagation of n-butanol/air and n-butanol/O2/He mixtures at pressures up to 20 atm, Combustion and Flame 191 (2018) 368-380.
[97] T. Knorsch, A. Zackel, D. Mamaikin, L. Zigan, M. Wensing, Comparison of different gasoline alternative fuels in terms of laminar burning velocity at increased gas temperatures and exhaust gas recirculation rates, Energy & fuels 28 (2014) 1446-1452.
[98] G. Broustail, P. Seers, F. Halter, G. Moréac, C. Mounaïm-Rousselle, Experimental determination of laminar burning velocity for butanol and ethanol iso-octane blends, Fuel 90 (2011) 1-6.
[99] M.V. Johnson, S.S. Goldsborough, Z. Serinyel, P. O'Toole, E. Larkin, G. O'Malley, H.J. Curran, A shock tube study of n-and iso-propanol ignition, Energy & Fuels 23 (2009) 5886-5898.
[100] I. Stranic, D.P. Chase, J.T. Harmon, S. Yang, D.F. Davidson, R.K. Hanson, Shock tube measurements of ignition delay times for the butanol isomers, Combustion and Flame 159 (2012) 516-527.
[101] C. Tang, L. Wei, X. Man, J. Zhang, Z. Huang, C.K. Law, High temperature ignition delay times of C5 primary alcohols, Combustion and Flame 160 (2013) 520-529.
[102] K. Heufer, J. Bugler, H. Curran, A comparison of longer alkane and alcohol ignition including new experimental results for n-pentanol and n-hexanol, Proceedings of the Combustion Institute 34 (2013) 511-518.
[103] K. Heufer, R. Fernandes, H. Olivier, J. Beeckmann, O. Röhl, N. Peters, Shock tube investigations of ignition delays of n-butanol at elevated pressures between 770 and 1250 K, Proceedings of the Combustion Institute 33 (2011) 359-366.
[104] B.W. Weber, K. Kumar, Y. Zhang, C.-J. Sung, Autoignition of n-butanol at elevated pressure and low-to-intermediate temperature, Combustion and flame 158 (2011) 809-819.